American Mineralogist, Volume 67, pages 696–717, 1982

Three-dimensional network structure of quenched melts (glass) in the systems SiO_2–$NaAlO_2$, SiO_2–$CaAl_2O_4$ and SiO_2–$MgAl_2O_4$

FRIEDRICH SEIFERT,[1] BJØRN O. MYSEN AND DAVID VIRGO

Geophysical Laboratory, Carnegie Institution of Washington
Washington, D. C. 20008

Abstract

The structures of quenched melts (glass) on the joins SiO_2–$NaAlO_2$, SiO_2–$CaAl_2O_4$ and SiO_2–$MgAl_2O_4$, inferred from Raman spectroscopic data, consist of interconnected, three-dimensional Si-, (Si,Al)- and Al-bearing tetrahedra. It is suggested that quenched SiO_2 and aluminosilicate melts with monovalent cations (Na^+) to charge-balance Al^{3+} in tetrahedral coordination may display a bimodal distribution of intertetrahedral angles in the three-dimensionally interconnected rings. The proportion of rings with the largest angle, and therefore the smallest *T*–O distance, decreases with increasing Al/(Al+Si) of the melt.

Quenched aluminosilicate melts with divalent cations (Ca^{2+} and Mg^{2+}) to charge-balance Al^{3+} in tetrahedral coordination probably consist of mixtures of three-dimensionally interconnected rings with no Al^{3+} (six-membered SiO_2-rings), rings with Al/Si = 1 (four-membered $Al_2Si_2O_8^{2-}$-rings) and rings with no Si^{4+} (six-membered AlO_2^--rings). The proportions of ring types in the melts depend on Al/(Al+Si).

Several physical properties (density, compressibility and viscosity) as well as thermochemical properties of glasses and melts are consistent with the suggested melt-structure models.

On the basis of the present data and information available in the literature, the distribution of three-dimensional structural units in natural magma can be calculated. It was found from these calculations, for example, that the more basic a magmatic liquid, the larger the proportion of Al-free SiO_2-rings relative to other three-dimensional network units in the melt.

Introduction

Interpretation of spectroscopic data of quenched silicate melts (glass) has led to the conclusion that the melt structure may be treated successfully in terms of anionic species characterized by the linkage of tetrahedra, that is, by the number of oxygens per tetrahedral unit not bonded to another tetrahedral cation (Brawer and White, 1975, 1977; Furukawa and White, 1980; Furukawa *et al.*, 1981; Verweij, 1979a,b; Mysen *et al.*, 1980). A ratio of NBO/*T* (where *T* represents the tetrahedrally coordinated cations) equal to 4 thus defines a monomer species; 3, a dimer; 2, a chain; and 1, a sheet. If NBO/*T* equals zero, all tetrahedra are interconnected *via* all four oxygens and a three-dimensional network structure is formed.

The bulk compositions of more than 95% of all natural magmas fall in the region of NBO/*T* between 1 and 0. From a petrological point of view, this range of NBO/*T* is, therefore, of particular interest. In this compositional interval, it has been suggested that three-dimensional network units are present in the melt (*e.g.*, Bockris *et al.*, 1955; Mysen *et al.*, 1981). In acidic magmatic liquids, for example, more than 75% of the anionic structure is made up of such units. Consequently, it is important to determine whether there is significant dependence on composition of the kind of three-dimensional structural units that might be found.

Even with a three-dimensional network structure, melts on aluminate–silica joins show variation in physical properties as a function of composition. For instance, the viscosity of melts decreases markedly with increasing Al/(Al+Si) along the joins SiO_2–$NaAlO_2$ (Riebling, 1966), SiO_2–$MgAl_2O_4$ (Riebling, 1964) and SiO_2–$CaAl_2O_4$ (Rossin *et al.*, 1964). Cranmer and Uhlmann (1981), on the basis of

[1]Present address: Mineralogisches–Petrographisches Institut und Museum, Universitat Kiel, Kiel, West Germany.

0003–004X/82/0708–0696$02.00

the viscous behavior of melts on the join $NaAlSi_3O_8$–$CaAl_2Si_2O_8$, suggested significant structural differences of the end-member melts. The pressure dependence of viscosity also is different in these systems. Whereas SiO_2–$NaAlO_2$ melts exhibit a significant viscosity decrease with increasing pressure (Kushiro, 1976, 1978), those in the SiO_2–$CaAl_2O_4$ system show little variation or even a viscosity increase with increasing pressure (Kushiro, 1981). The data of Kushiro (1978, 1981) also show that the compressibility of melts with Na^+-charge-balanced Al^{3+} is considerably greater than those with Ca^{2+} charge-balanced Al^{3+} but with the same Al/(Al+Si).

Flood and Knapp (1968) suggested that the crystal-liquid phase equilibria on the join $NaAlSi_3O_8$–$CaAl_2Si_2O_8$ may be explained by invoking several coexisting compositionally different structural units in the melts. Structural dissimilarity of the end-member and mixed compositions on this join have also been suggested from X-ray radial distribution (Taylor and Brown, 1979a) and thermochemical (Navrotsky *et al.*, 1980) data.

Because of observations such as those summarized above, the present study was carried out to examine the structural details of quenched melts in the systems SiO_2–$NaAlO_2$, SiO_2–$CaAl_2O_4$ and SiO_2–$MgAl_2O_4$. In view of infrared Raman and X-ray radial distribution data on compositions above the glass transition point and in the molten state (Sweet and White, 1968; Seifert *et al.*, 1981; Taylor *et al.*, 1980), it is suggested that the data may also apply to important structural features of molten silicates. The data will help to formulate the relationship between melt structure and physical properties of silicate melts and magmas with a significant abundance of three-dimensional structural units.

Experimental techniques

Homogeneous glasses were prepared from spectroscopically pure SiO_2, MgO, $CaCO_3$, Na_2CO_3 and Al_2O_3 by melting thoroughly ground mixes of 200–400 mg at temperatures of 1550–1660°C for 1–4 hr and quenching in air. Table 1 provides a list of electron microprobe analyses and nominal compositions of the starting materials.

Raman spectra have been taken from glass chips about 2–3 mm across irradiated with an 8 watt argon-ion laser (wavelength 488.0 nm) with a 90° scattering geometry. Other spectroscopic details have been reported by Mysen *et al.* (1981, 1980).

The high input power (about 3–4 watts at the sample on an area about 0.5 mm across) results in local heating of the glass chips. Comparison of Stokes to anti-Stokes intensities (*cf.*, Long, 1977) indicates that this heating is 100±25°C, which has been taken into account in the temperature reduction process of the data (see below). The spectra were recorded at 1 cm^{-1} intervals with a Jobin–Yvon optical system, holographic grating, double monochromator (HG25) and a digitized photon-

Table 1. Analyzed and nominal (parentheses) compositions of prepared samples and density of their glasses at 20°C

Sample	SiO_2	Al_2O_3	Na_2O	CaO	MgO	Al/(Al + Si)	Density, g/cm^3
SAN	83.14(83.69)	10.22(10.14)	6.11(6.17)	-	-	0.125	ND*
AS50	73.95(74.57)	15.85(15.81)	9.65(9.62)	-	-	0.200	ND
Ab	68.90(68.74)	19.30(19.44)	11.52(11.82)	-	-	0.250	2.28
Jd	59.85(59.45)	24.93(25.22)	14.93(15.33)	-	-	0.333	2.33
Ne	42.40(42.30)	35.60(35.88)	21.70(21.85)	-	-	0.500	2.58
CA214	83.90(84.18)	10.20(10.21)	-	5.56(5.61)	-	0.125	2.28
CA2S8	74.88(75.26)	15.95(15.96)	-	8.65(8.78)	-	0.200	2.33
CA2S6	69.00(69.52)	19.55(19.67	-	10.74(10.81)		0.250	ND
CA2S4	60.30(60.33)	25.72(25.60)	-	14.22(14.07)		0.333	2.45
CA2S2	43.24(43.19)	36.40(36.65)	-	20.25(20.16)		0.500	2.66
CATS	27.43(27.53)	46.70(46.74)	-	24.64(25.71)		0.667	2.76
CA6S4	11.56(11.25)	58.19(57.26)	-	30.41(31.49)	-	0.750	ND
$CaAl_2O_4$	-	65.12(64.52)	-	35.50(35.48)		1.000	ND
MA2S14	85.19(85.53)	10.35(10.37)	-	-	4.08(4.10)	0.125	ND
MA2S8	77.50(77.16)	16.25(16.37)	-	-	6.44(6.47)	0.200	2.27
MA2S6	71.70(71.70)	20.17(20.28)	-	-	8.72(8.02)	0.250	2.35
MA2S4	62.12(62.82)	26.74(26.65)	-	-	10.50(10.53)	0.333	2.49
MA2S2	45.62(45.79)	38.74(38.85)	-	-	15.22(15.36)	0.500	ND

*Not determined.

counting detection system (for detailed description see Mysen *et al.*, 1982a).

After a background and temperature correction, the data were fitted to Gaussian lines. Mysen *et al.* (1982a) described these procedures in detail, and only a brief summary is provided here. Before curve-fitting, the digitized data were corrected for intensity- and temperature-dependence of the scattered intensity. In the present experiments, in which only relative intensities have been considered, a factor, R, of the form employed by Long (1977) is used:

$$R = \nu_0^3[-\exp(-hc\nu/RT) + 1]\nu/(\nu + \nu_0)^4 \quad (1)$$

where ν_0 and ν are the frequencies of the exciting line and the Raman shift, respectively. In order to obtain a corrected spectrum, the measured intensities were multiplied by R.

There is a nearly linear instrumental 1–2° positive background slope in the frequency range between 800 and 1300 cm^{-1}. A background slope beneath the high frequency envelopes (usually between 800 and 1250 cm^{-1}) was determined by least squares regression of a straight line to the data beginning about 100 cm^{-1} to about 300 cm^{-1} above the high-frequency tail of the high-frequency envelope and extrapolated beneath the high-frequency envelope.

The quality of the fit was determined with the aid of χ^2 and the randomness of the residuals. The χ^2 is the sum of the squares of the differences between the calculated (from fitted lines) envelope and the data points. The absolute value of χ^2 is, therefore, both a measure of the deviations from a perfect match and the scatter in the data point of different fits to a given spectrum. The greater the deviation or the greater the scatter, the larger is the value of χ^2. For this reason the values of χ^2 are only meaningful when comparing different fits of a given set of data.

The χ^2 does not indicate whether certain parts of a given spectrum are poorly fitted. Such features will appear as nonrandomness of the residuals. These considerations in combination are used to determine the quality of a fit.

Even with these statistical tests, a solution is not necessarily unique. When non-unique situations develop, other information such as internal consistency with regard to inferred structural models or other compositional trends in properties, or both, are also considered to decide which fit is preferred. An example of such a situation is the fit to the spectrum of quenched melt of $NaAlSi_3O_8$ composition (see below).

In fitting all the spectra it is also assumed that individual bands are symmetric and that they may be described with Gaussian lines. Walrafen (1967) suggested that spectra of an amorphous substance like H_2O may be fitted with symmetric Gaussian lines. Hartwig (1977) made similar suggestions for water-bearing vitreous SiO_2. Baker and Sievers (1975) suggested that Raman bands from glassy substances might be described as Gaussian distributions of Lorentzian bands. An example of a few fits with Gaussian and Lorentzian line-shapes to the high-frequency portion of the spectrum of vitreous SiO_2 is given in Figure 1. These fits illustrate the main two problems with Lorentzian line shape in curve-fitting of Raman spectra of silicate glasses. First, Lorentzian lines have broad shoulders that cannot be fitted to the shoulders of Raman bands from glasses. Second, the Lorentzian lines tend to be too sharp near their maxima. These problems are also evident in the larger values of χ^2 of Lorentzian as compared with Gaussian line shapes. Mysen *et al.* (1982a) in describing the method used here also concluded that Raman spectra of a broad bulk compositional range of binary metal oxide–silica quenched may be fitted to Gaussian lines. The structural model thus created is internally consistent, and aids to explain physical properties of melts as well as phase equilibria (Mysen *et al.*, 1982b).

Independent tests for the line shapes and symmetries are not available. For example, theoretical calculations of spectra on the basis of density of states depend on the structural model used. Bell and Dean (1972) showed asymmetric distribution of the density of states for vitreous SiO_2 with the assumption of a single random distribution of the ions. Thus asymmetric Raman bands may follow. Gaskell (1975) and Gaskell and Mistry (1975) with the aid of high-resolution electron microscopy suggested, however, that more than one structure type may be found in vitreous SiO_2. The results from molecular dynamics calculations by Soules (1979) and Gaskell and Tarrant (1980) showed asymmetry of the distribution of Si–O–Si angles in vitreous SiO_2. This observation is also consistent with more than one structure. It is not at all clear, therefore, whether available data even for a chemically relatively simple compound like SiO_2, can be used to test the assumptions in the present fitting routine. We assume that the Raman bands for disordered substances such as silicate glass (and melt) are

symmetric and can be described with Gaussian-like shapes. The success of the method at present is assessed with the consistency of the inferred structural models, their relative simplicity, and the ability of the structural model to explain and predict chemical and physical properties of the materials studied.

The number of lines fitted to individual spectra was limited to the point where additional lines did not result in statistically significant improvement of χ^2 and in the randomness of the distribution of the residuals. The parameters derived for such fits are precise to within ± 10 cm^{-1} in line position and half width and about 10% (relative) in intensity and area for bands with relative area greater than about 20%. For the relative area range 5–20%, the relative uncertainty is near 25%, and for bands with less than 5% relative area, the uncertainty ranges between 25 and 50%.

For a number of samples the glass density has

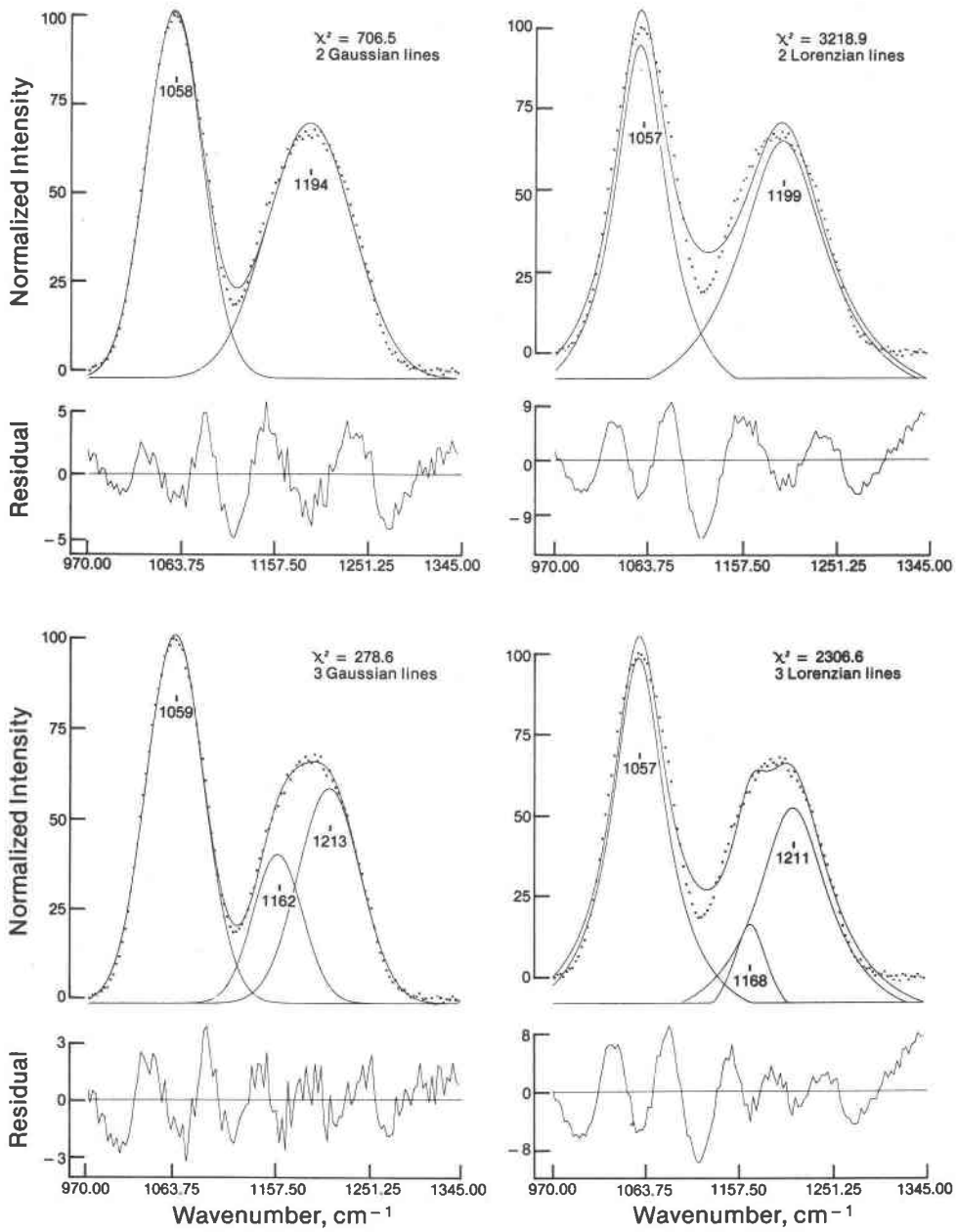

Fig. 1. Fitted Gaussian and Lorentzian lines to high-frequency portion of unpolarized spectrum of vitreous SiO_2.

been determined on chips of 10–30 mg weight with a Berman balance and toluene as an immersion medium. The accuracy achieved is about ± 0.02 g/cm^3. The density data are also listed in Table 1.

Experimental results

SiO_2

The unpolarized spectrum of vitreous SiO_2, corrected for temperature- and frequency-dependent scattering efficiency (equation 1) is shown in Figure 2. The spectrum consists of a low-frequency region with distinctive bands at 440, 495 and 605 cm^{-1}. In the high-frequency range, vitreous SiO_2 exhibits three visually resolved peaks centered at 810, 1060 and 1195 cm^{-1}. This spectrum does not differ from that of other investigators. The fitting process and the statistical tests applied lead us to suggest, however, that more than three peaks are required in this spectral region in order to fit the data adequately. The asymmetric peak at 810 cm^{-1} has to be split into two Gaussian bands at 793 and 829 cm^{-1}. Residual intensity in the region between 810 and 1000 cm^{-1} necessitates the introduction of another peak at about 900 cm^{-1}. Finally, the fit is markedly improved in the region 1100–1300 cm^{-1} by splitting the rather broad band at 1195 cm^{-1} into two bands. Examples for the different fits are given in Figure 2.

SiO_2–$NaAlO_2$

In addition to SiO_2, four samples have been studied on this join extending to the nepheline composition (*i.e.*, Al/(Al+Si) = 0.5). The low-frequency region resembles that of SiO_2 but becomes less well resolved, and the 605 cm^{-1} and 900 cm^{-1} bands in vitreous SiO_2 shift to lower frequency with increasing Al/(Al+Si) (Fig. 3).

Visually, the resolution of the high-frequency

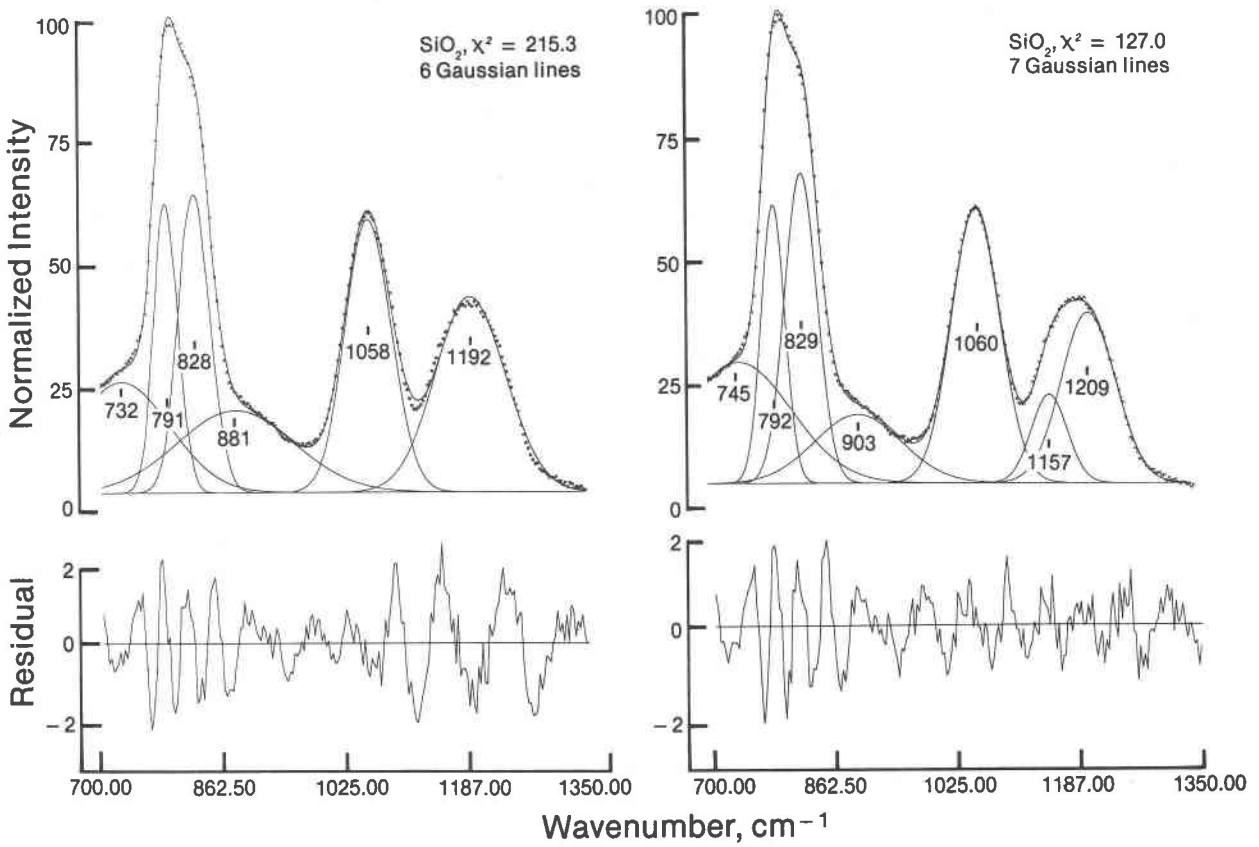

Fig. 2. High–frequency portion of the unpolarized Raman spectrum of vitreous SiO_2 fitted to different numbers of Gaussian bands. Intensities (percent) are normalized to the strongest band in the displayed spectrum. Squares represent measured data points averaged over 3 cm^{-1} (each observation is at 1 cm^{-1}). The curves indicate the individual Gaussian bands fitted as well as their sum curve. The deviations between the sum fitted curve and the observed spectrum are plotted as residuals below the spectra. The χ^2 values and the total number of lines are also given. Note the improvement in the χ^2 value and the distribution of residuals with increasing number of lines. The spectrum with the lowest χ^2 value and the more random distribution of residuals is the one used in the interpretation.

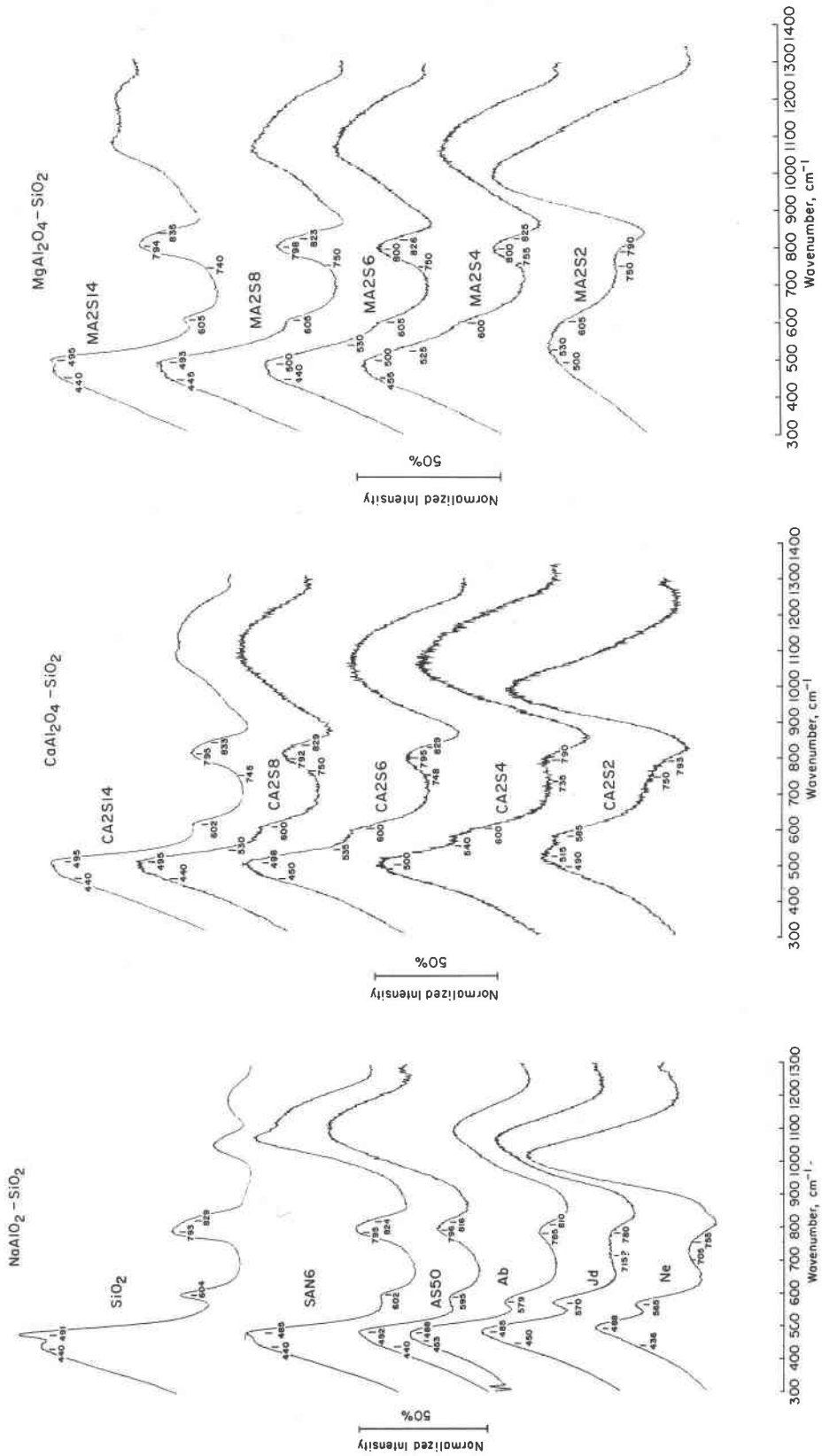

Fig. 3. Raman data (corrected for temperature- and frequency-dependent scattering efficiency) of melts on the joins $NaAlO_2$–SiO_2, $CaAl_2O_4$–SiO_2 and $MgAl_2O_4$–SiO_2.

portion of the spectrum as seen in SiO_2 decreases with even small additions of $NaAlO_2$ component. The broad envelope thus generated gradually moves toward lower frequencies with increasing Al content. The number of lines to be fitted to such an unstructured envelope may not be self-evident, and Figure 4 shows a series of fits to the AS50 and albite composition spectra with different numbers of Gaussian lines under the envelope.

The distribution of residuals becomes more random as the number of lines is increased and, more importantly, there is a significant reduction in the χ^2 value. Inclusion of additional lines beyond those shown does not improve the χ^2 value and is therefore not considered statistically significant (Mysen *et al.*, 1982a). The five- and six-line fits of the spectra from quenched Ab melt are statistically indistinguishable. It will be suggested below that the six-line fit is more reasonable on the basis that the inferred structure of quenched melts on this join shows a gradual change with Al/(Al+Si) of the glass. With a five-line fit, the spectrum of quenched Ab-melt does not follow the structural trends indicated by the other compositions on the join $NaAlO_2$–SiO_2.

The fitted high-frequency envelopes of the spectra of quenched melts on the join $NaAlO_2$–SiO_2 are displayed in Figure 5. Starting from SiO_2, the high-frequency portion of the spectra exhibit a continuous shift of the high-frequency Raman bands toward lower frequencies (Fig. 6) and concomitant changes in band intensities (Fig. 7). Similar frequency trends have been observed in other Al-bearing systems (*e.g.*, Brawer and White, 1977; Mysen *et al.*, 1981). The 1209 cm^{-1} line of vitreous SiO_2 diminishes on increase of $NaAlO_2$ component, the 1157 cm^{-1} line increases in relative intensity, and the line at 1058 cm^{-1} splits into two bands. The doublet near 800 cm^{-1} shifts to slightly lower frequency, and the two bands near 800 cm^{-1} become less well resolved with increasing $NaAlO_2/SiO_2$.

SiO_2–$CaAl_2O_4$

On this join the range of samples from Al/(Al+Si) = 0 to 1 was prepared. At Al/(Al+Si) higher than 0.5 (= anorthite composition) the fitting of the spectra becomes increasingly difficult due to broad low-frequency bands whose tail regions extend under the high-frequency bands. The fitted spectra are shown in Figure 8. In the low-frequency range (Fig. 3) the 440 cm^{-1} band becomes less intense relative to the band in vitreous SiO_2 with increasing Al/(Al+Si). This band cannot be detected in the compositional range between CA2S6 and CA2S4. A new band between 510 and 540 cm^{-1} first appears in CA2S8 and becomes more intense with increasing Al/(Al+Si) (Fig. 3). There is also a broad band near 750 cm^{-1} in all the Al-bearing spectra from quenched melts on this join.

In contrast to the high-frequency bands in the Raman spectra of quenched melts on the SiO_2–$NaAlO_2$ join where line-frequencies shift systemati-

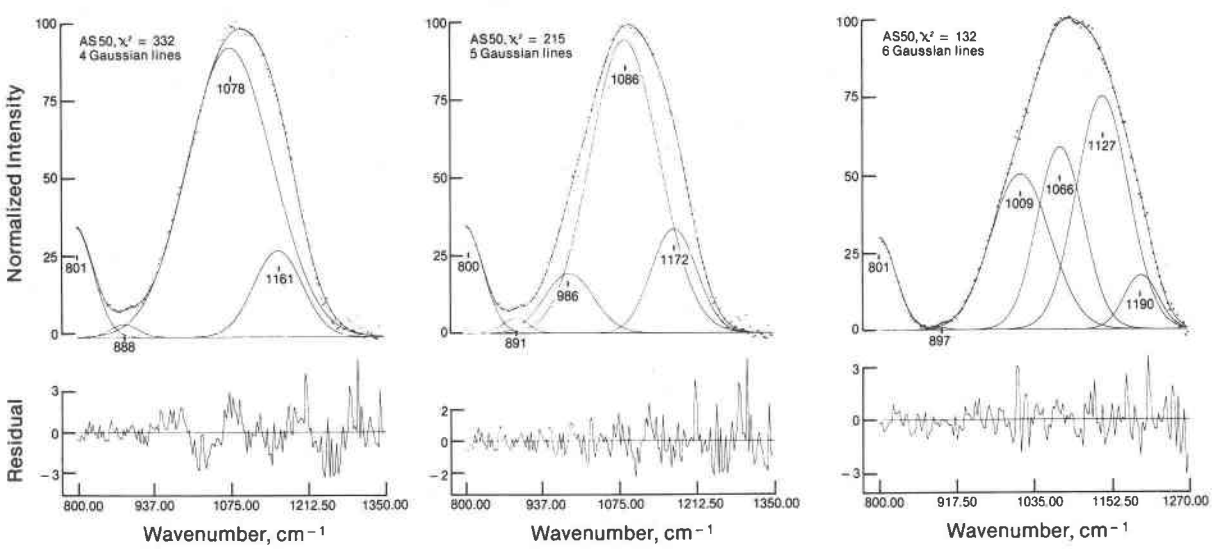

Fig. 4a. High–frequency part of unpolarized Raman spectra of glass of AS50 composition fitted to different numbers of Gaussian bands. See text and Figure 2 for discussion of procedures.

cally with bulk composition, the frequencies of the bands observed in SiO_2 remain essentially unaffected along the join SiO_2–$CaAl_2O_4$ with increasing Al/(Al+Si) (Fig. 9). Their relative intensities, however, vary systematically with increasing Al contents of the melts (Fig. 10). At the anorthite composition, the band near 1210 cm^{-1} can no longer be detected. The 1157 cm^{-1} band cannot be observed at Al/(Al+Si) > 0.67 (CATS).

Addition of small amounts of $CaAl_2O_4$ component (12.5 mole %) to SiO_2 produces additional bands at about 980 and 920 cm^{-1}. In the siliceous samples, the 920 cm^{-1} band is poorly resolved and probably contains a contribution from the 903 cm^{-1} band found in SiO_2. The extent of this contribution could not, however, be determined. The 980 cm^{-1} band becomes the most intense feature of the high-frequency envelopes at intermediate Al contents

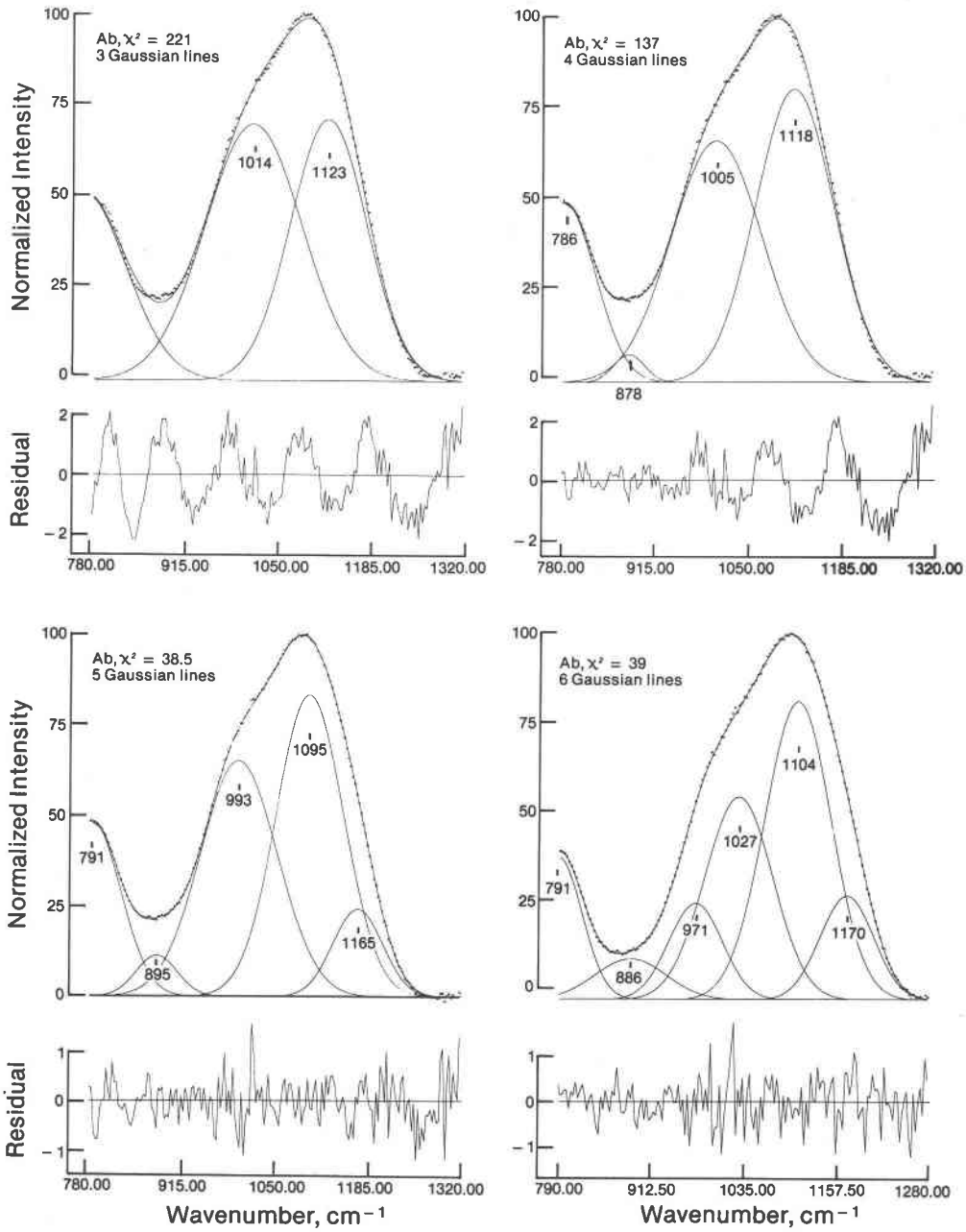

Fig. 4b. High-frequency part of unpolarized Raman spectra of Ab composition fitted to different numbers of Gaussian bands. See text and Figure 2 for discussion of procedures.

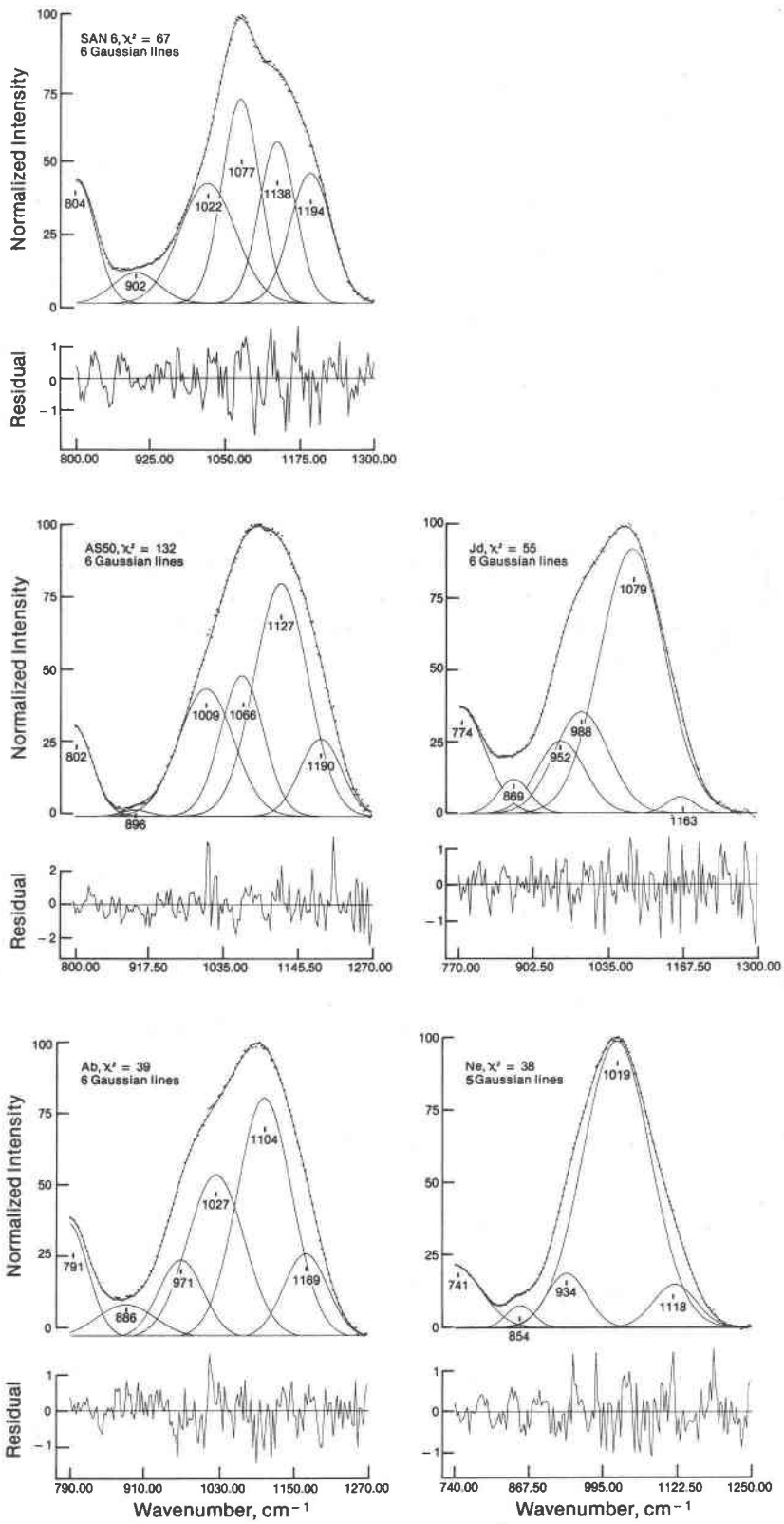

Fig. 5. High–frequency part with best Gaussian fits of the unpolarized Raman spectra of compositions on the join SiO_2–$NaAlO_2$.

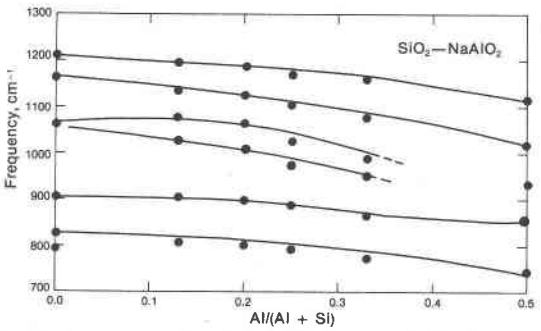

Fig. 6. Frequency of relevant Raman bands in the system SiO_2–$NaAlO_2$ as a function of Al/(Al+Si) of the glass.

(*i.e.*, close to the anorthite composition; see Fig. 8). Neither the 980 nor the 920 cm^{-1} band could be detected in the spectrum of the vitreous $CaAl_2O_4$ end-member. The two high-frequency bands of vitreous $CaAl_2O_4$, *i.e.*, the 871 and 778 cm^{-1} bands, occur in the spectra of the less siliceous samples of the SiO_2–$CaAl_2O_4$ join and can be traced back, with decreasing intensity, to the anorthite composition. The line parameters of these bands are particularly uncertain, however, due to the overlap with tails of the low-frequency bands.

SiO_2–$MgAl_2O_4$

The Raman spectra of quenched melts on this join, which was studied up to Al/(Al+Si) = 0.5, exhibit spectral features similar to those on the SiO_2–$CaAl_2O_4$ join (Figs. 3, 8–13), that is, constancy of line positions and systematic intensity changes as a function of $MgAl_2O_4/SiO_2$ (Figs. 12 and 13). The low-frequency portions of these spectra are also similar to those on the join $CaAl_2O_4$–SiO_2 (Fig. 3). They differ in detail, however, in that the compositional range where the 440 cm^{-1} band is detected extends to higher values and the 510–540 cm^{-1} band extends to lower values of Al/(Al+Si) than in the system $CaAl_2O_4$–SiO_2.

The positions of the new bands appearing in the MA2S14 composition near 980 and 910 cm^{-1} match closely those encountered on the SiO_2–$CaAl_2O_4$ join (Figs. 8 and 11). In the MA2S2 composition (equivalent to anorthite in the system SiO_2–$CaAl_2O_4$) a new band appears near 870 cm^{-1}. In contrast to the spectra of quenched melts of analogous compositions on the join SiO_2–$CaAl_2O_4$, where the 1200 cm^{-1} band disappears in the compositional range of Al/(Al+Si) betweem 0.33 (CA2S4) and 0.5 (An), the 1200 cm^{-1} band also occurs in MA2S2 glass Al/(Al+Si) = 0.5 (see Figs. 8 and 11).

Interpretation and discussion of data

SiO_2

Compositionally, SiO_2 is the simplest chemical compound relevant to the structure of petrologically important silicate melts. Its structure has been studied with the aid of theoretical molecular dynamics calculations, by X-ray methods and by spectroscopic techniques.

There is general agreement that molten SiO_2 may be best described as a three-dimensional network, but the details of the structure remain open to discussion. Bell and Dean (1972) suggested that a random network model may be used to describe a number of spectroscopic features as well as RDF data. The resulting calculated Raman spectrum does, however, show most bands 50 cm^{-1} or more lower than the actual positions. Recent refinements by Gaskell and Tarrant (1980) and Soules (1979) indicate that in vitreous SiO_2, the distribution of values of the Si–O–Si angle is asymmetric. This asymmetry may be explained by the existence of more than one 3-dimensional unit in the melt. High-resolution electron microscopy (Gaskell, 1975; Gas-

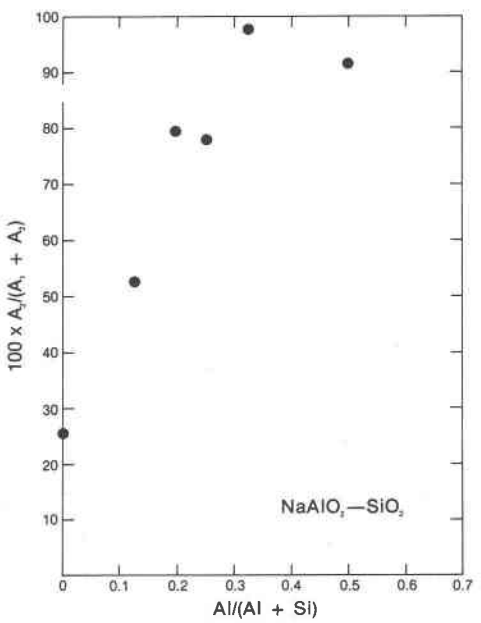

Fig. 7. Proportion of areas A_1 (W4; unit I) and A_2 (W4; unit II) relative to their total area in melts on the join SiO_2–$NaAlO_2$ (Al and A2; Table 2). These two bands are chosen to illustrate the relative changes of unit I and unit II type six-membered rings in the system. If it is assumed that the relative scattering power of the vibrations responsible for these bands is independent of Al content of the unit, the area proportion corresponds to the proportion of the relevant structural unit in the melt.

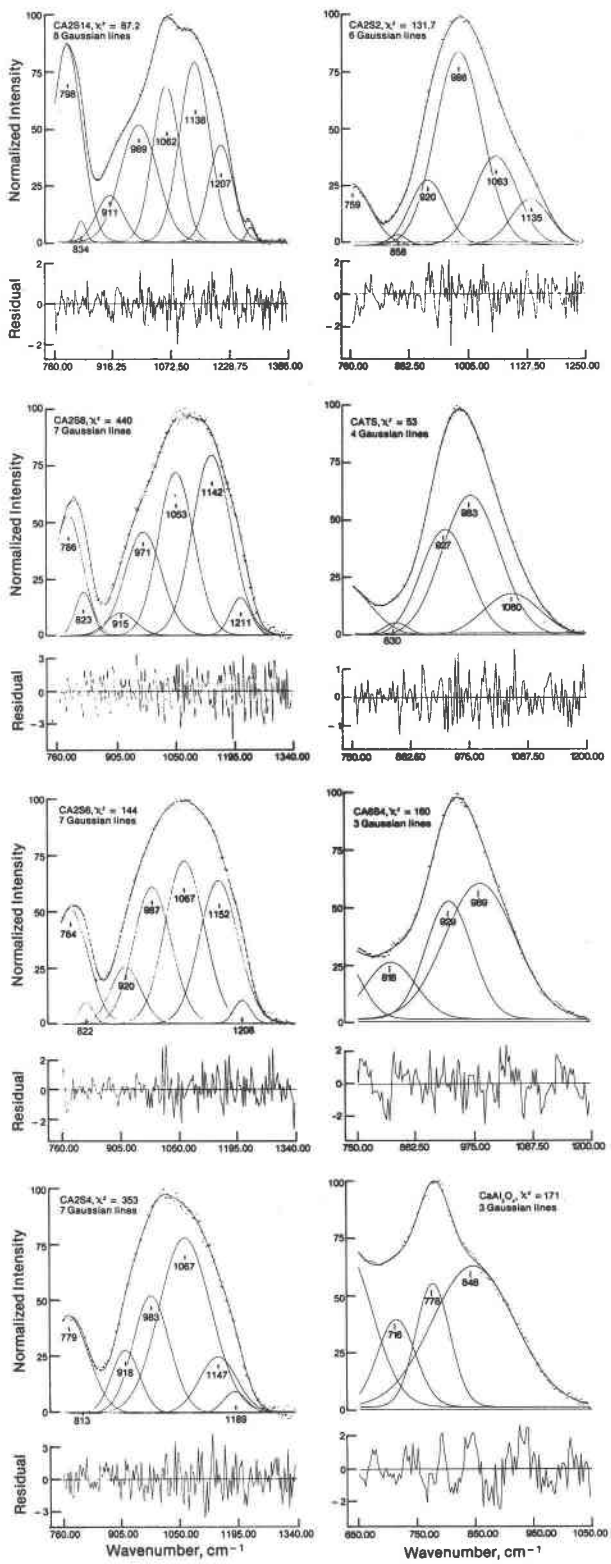

Fig. 8. High-frequency part of the unpolarized Raman spectra of glasses on the join SiO_2–$CaAl_2O_4$ together with the statistically best fit of Gaussian lines. The small peak that sometimes occurs near 1280 cm^{-1} is attributed to C–O stretching from CO_2 of trapped air in the samples.

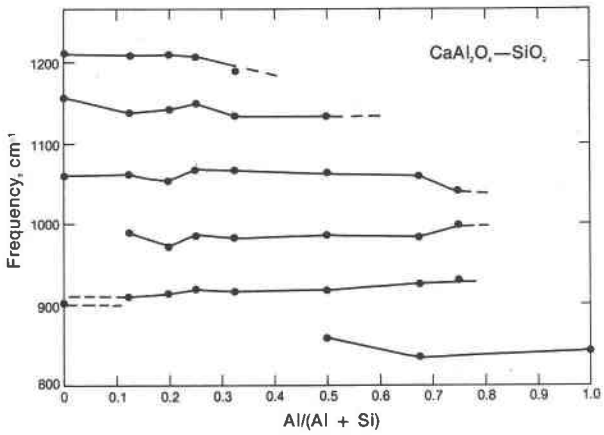

Fig. 9. Frequency of relevant Raman bands in the system SiO_2–$CaAl_2O_4$ as a function of bulk Al/(Al+Si) of the glasses.

kell and Mistry, 1979; Bando and Ishizuka, 1979) also indicates that vitreous SiO_2 consists of at least two distinct structures.

The Raman spectroscopic data (*e.g.*, Figs. 2 and 3) cannot easily be interpreted on the basis of a single structure unless concepts such as longitudi-

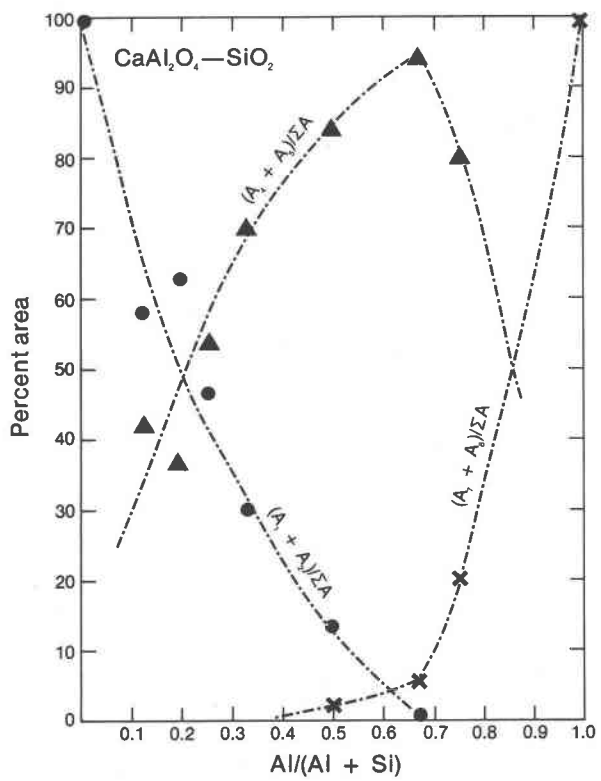

Fig. 10. Proportion of areas of bands stemming from the different structural units in melts on the join SiO_2–$CaAl_2O_4$ as a function of bulk Al/(Al+Si) of the glasses. In this figure $A_1 + A_2$ corresponds to 1210 cm^{-1} + 1160 cm^{-1} bands in six-membered SiO_2 rings. $A_4 + A_5$ corresponds to 980 cm^{-1} + 910 cm^{-1} bands in $Al_2Si_2O_8^{2-}$ four-membered rings. $A_7 + A_8$ represents the corresponding bands for six-membered $Al_2O_4^{2-}$ rings.

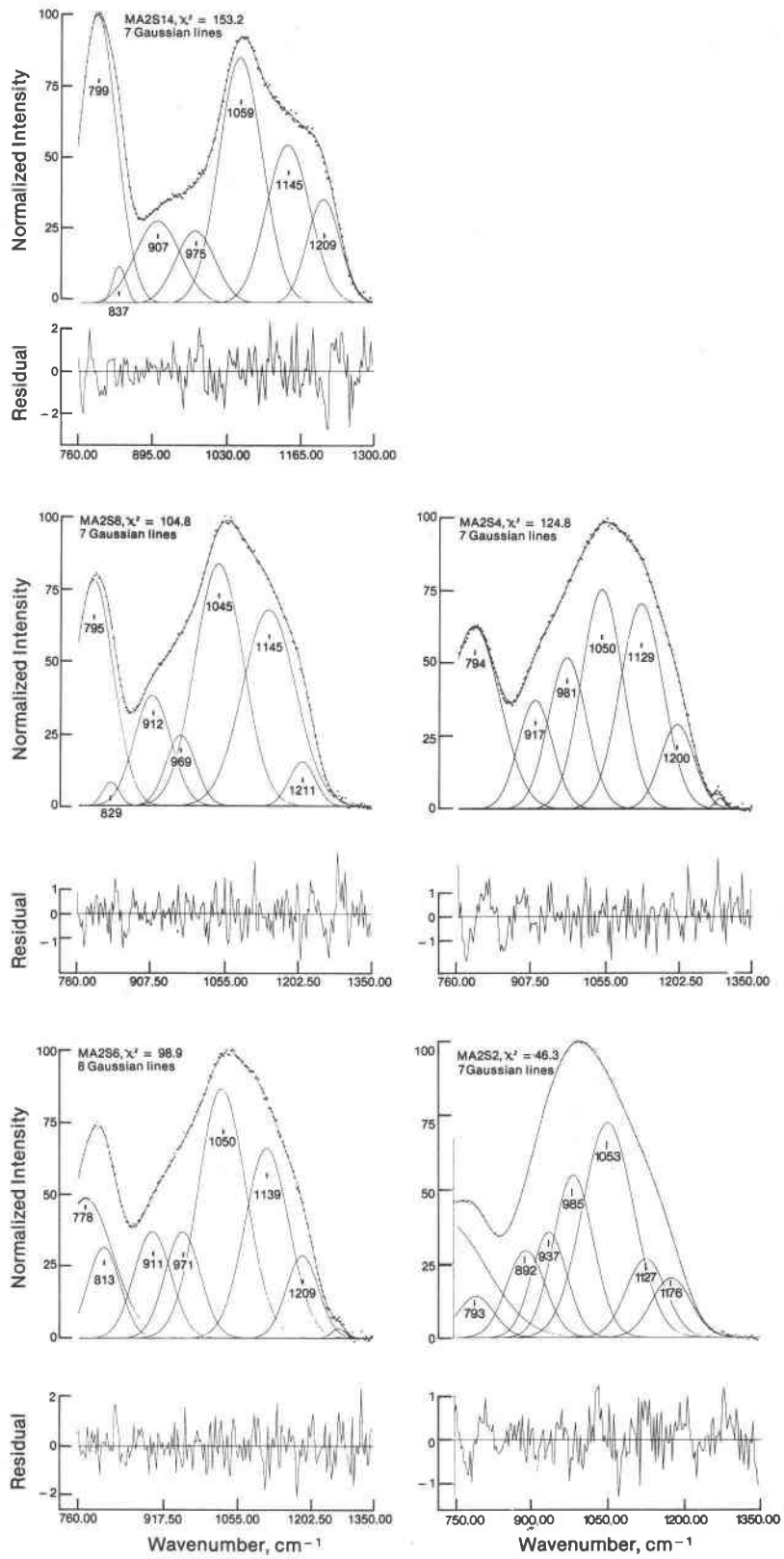

Fig. 11. High-frequency portion of unpolarized Raman spectra of glasses on the join SiO_2–$MgAl_2O_4$.

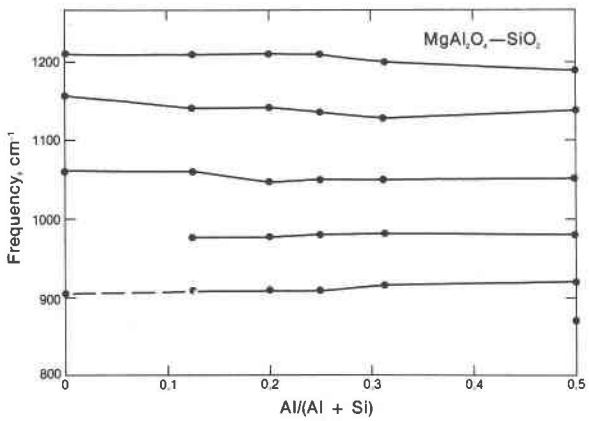

Fig. 12. Frequency of relevant Raman bands in the system SiO_2–$MgAl_2O_4$ as a function of bulk Al/(Al+Si).

nal optical (LO) and transverse optical (TO) splitting (*e.g.*, Galeener and Lucovsky, 1976), involving long-range order in amorphous SiO_2, are invoked. Furthermore, LO and TO splitting do not aid in explaining the results derived by Soules (1979) and Gaskell and Tarrant (1980) where more than one average Si–O–Si angle may be suggested.

The Raman spectroscopic data may, however, be interpreted on the basis of two structural units, which differ in Si–O–Si angle. Mammone *et al.* (1981) suggested that two structures, one with an interconnected four-membered and one with an interconnected six-membered ring may be used to explain their Raman spectroscopic data. This suggestion may explain the skewed Si–O–Si angle distribution observed by Gaskell and Tarrant (1980). It is also in agreement with the TEM data by Gaskell and Mistry (1975).

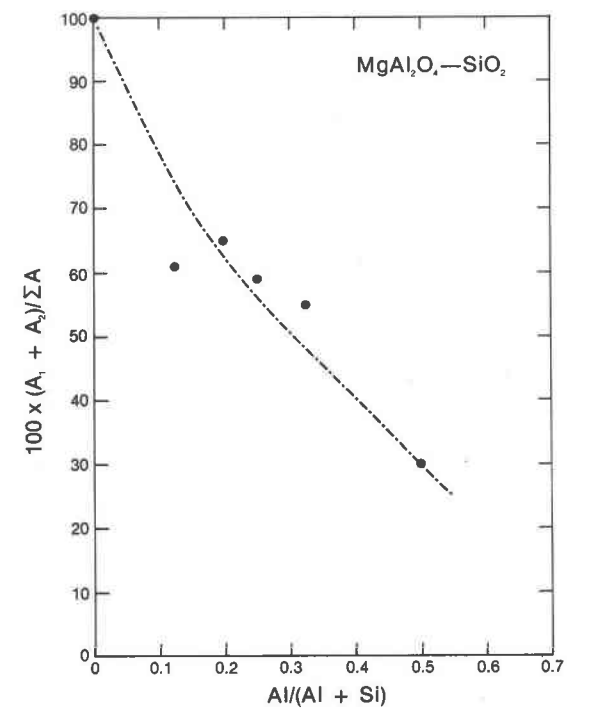

Fig. 13. Area ratios in the system SiO_2–$MgAl_2O_4$. For discussion and notations see Figure 10 and text.

Mammone *et al.* (1981) did not provide data as to why four- and six-membered rings were chosen. Their data as well as those chosen here are, however, consistent with the existence of more than one (probably two) different average Si–O–Si angles.

A simplified model that may be applied to assess whether the doublets in the Raman spectra represent two structures with different Si–O–Si angles is the central-force model (Sen and Thorpe, 1977; Galeener, 1979; Thorpe and Galeener, 1980). In this model, it was assumed (*e.g.*, Galeener, 1979) that the force constants of bending and rocking modes in AX_2 tetrahedral glasses are essentially zero. The stretching modes are the only ones considered. For the A–X–A (Si–O–Si) angle (θ) at 90°, only two modes (A_1 and A_2) will be observed. With greater values of θ, the A_1 (at the lowest frequency) splits into a band of states limited by a low frequency, W1, and a band of states at higher frequency (W2). The A_2 mode splits into a lower frequency, W3, a higher frequency, W4, and a band of states in between. The frequencies of the maxima in the density of states depends on the force constant, α, and the inter-tetrahedral angle, θ (Sen and Thorpe, 1977):

$$W1^2 = (\alpha/M_A)(1 + \cos\theta), \quad (2)$$

$$W2^2 = (\alpha/M_X)(1 - \cos\theta), \quad (3)$$

$$W3^2 = W1^2 + (4\alpha)/3M_A, \quad (4)$$

and

$$W4^2 = W2^2 + (4\alpha)/3M_A, \quad (5)$$

where M_A and M_X are the atomic weights of the atoms. By using cm^{-1} as frequency (instead of rad/sec), $\alpha = \alpha/0.0593$ (dyn/cm).

Galeener (1979) found that for vitreous SiO_2, GeO_2 and BeF_2, this model resulted in calculated spectra very similar to those of Bell and Dean (1970) from their larger-cluster calculations despite the fact that Galeener (1979) did not include a non-central force constant. The calculated spectra did, as did those of Bell and Dean (1972) seem to require LO- and TO-splitting to account for all the observed

features. We will attempt to use the same model with the difference that the structures of the three-dimensional glasses may consist of at least two maxima in Si–O–Si or (Si,Al)–O–(Si,Al) angles.

In the central force model 1160 (1210), (793) and 440 (490) cm^{-1} bands may be denoted W4, W3 and W1 vibrations, respectively. The numbers in parentheses refer to positions of the postulated second structural type in vitreous SiO_2. The W2 band is at 1060 cm^{-1} in vitreous SiO_2.

The bands near 600 cm^{-1} and 900 cm^{-1} commonly have been assigned to broken Si–O bonds in the network (Bates *et al.*, 1974; Stolen and Walrafen, 1976; Lucovsky, 1979). The defect density corresponds to about 0.1% of the bridging oxygen bonds in the structure (Seifert *et al.*, 1981).

The Si–O–Si angle and force constants may be calculated from the frequencies of W4 and W3 (Galeener, 1979) as shown in Table 2. The lower band limit of W2 and calculated frequency of W1 are also included. The agreement between calculated W1 and W2 (limit) (Galeener, 1979) and observed positions lends credence to the structural model for vitreous SiO_2. As also pointed out by Galeener (1979), the θ-values are about 10° too low. This discrepancy is probably due to the simplifying assumptions in the application of the central-force model (Galeener, 1979).

The set of smaller Si–O–Si angles is associated with the smaller force constant, a result that may imply larger Si–O distances than in the unit with the larger Si–O–Si angle. Such an inverse relationship between Si–O distances and Si–O–Si angles has also been found by Hill and Gibbs (1979) in crystalline silica and silicates. The observation of two different force constants is also in agreement with the suggestion of deJong and Brown (1980) that a bimodal Si–O–Si angle distribution in vitreous SiO_2 can be expected only if the Si–O distances also show a bimodal distribution.

With this interpretation of the spectrum of SiO_2, the half-widths of the function describing the distribution of Si–O–Si angles in the two sets are comparable to the differences between the two sets. In other words, there is strong overlap between them, and a histogram of all Si–O–Si angles taken together would not show an intermediate minimum but only one asymmetric envelope, similar to that derived by Gaskell and Tarrant (1980) and Soules (1979). According to the present interpretation of the data, this frequency distribution would be skewed toward lower Si–O–Si angles, as calculated by Soules (1979). The difference in average Si–O–Si angles between the two sets (5°) compares favorably with that postulated by Vukcevitch (1972; 8°) on the basis of physical properties. We suggest, therefore, that the central-force model can give sensitive information on differences or relative changes of bond angles and bond lengths in silicate glasses (and presumably melts) with an interconnected, three-dimensional structure. The available data cannot be used to determine the average number of Si^{4+} in these rings. It has been suggested that the structure of glassy SiO_2 consists of six-membered rings (Konnert and Karle, 1973; Taylor and Brown, 1979b; Navrotsky *et al.*, 1980). We suggest that there may be two types of six-membered rings where "puckering" of one of them leads to an Si–O–Si angle maximum 5–10° smaller than the other one.

Table 2. Derived parameters for the two structural units in samples along the join SiO_2–$NaAlO_2$

	SiO_2	SAN6	AS50	Ab	Jd	Ne
			Unit I			
θ	132.0	131.5	131.6	131.2	133.1	133.8
α	569.9	557.1	553.5	534.8	523.1	480.5
W2 (limit)	1001	988	985	967	963	926
W1	500	501	496	499	472	467
			Unit II			
θ	127.0	126.1	125.4	124.7	124.5	123.2
α	536.8	522.3	514.0	494.8	472.3	424.0
W2 (limit)	952	935	925	905	883	831
W1	430	433	436	431	426	415
θ_{av}	130.7	128.7	126.7	126.1	124.7	124.1

θ = Intertetrahedral (T–O–T) angle.
α = Force constant (N/m).
W2 = Calculated band edge of the W2 vibration (cm^{-1}).
W1 = Calculated frequency of W1 from observed W4 and W3.
θ_{av} = Weighted mean intertetrahedral angle (see text).

SiO_2–$NaAlSiO_2$

The continuous shift of line frequencies of the spectra from quenched melts along this join (Figs. 3, 5, and 6) and the absence of any additional bands as Al/(Al+Si) is increased (except for the splitting of the 1060 cm^{-1} band in SiO_2) lead us to suggest that the structure of the SiO_2 framework is largely preserved when $NaAlO_2$ is incorporated in the network. It is implied, therefore, that Al^{3+} is incorporated mainly in six-fold rings of SiO_2 and that the two different structures postulated above for vitreous SiO_2 are also present in the NaAl-bearing glasses.

The force constant and the *T*–O–*T* angle for both types of structural units may be calculated (Table

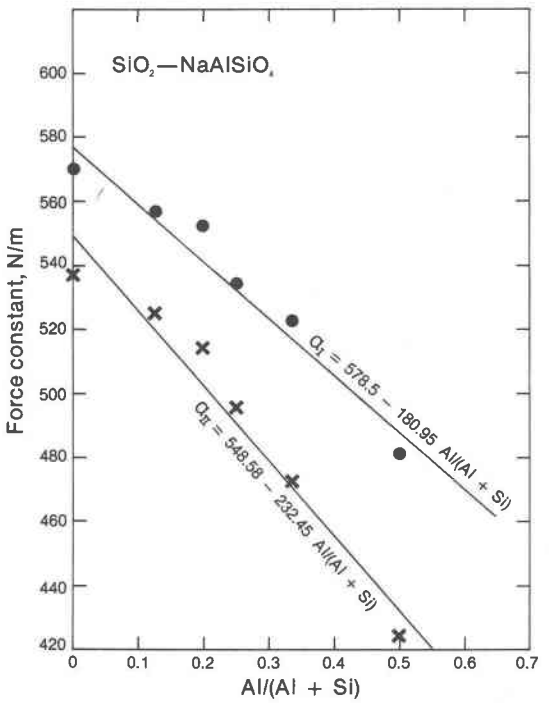

Fig. 14. Force constants (*N/m*)*versus* Al/(Al+Si) of the two units in the system SiO_2–$NaAlO_2$.

2). In these calculations, it was assumed that Al/(Al+Si) was the same in both structural units. The uncertainty introduced by the unknown value of Al/Si of each postulated unit (M_A in equations (2–5) may be anywhere between 27 and 28) results in only ~1% uncertainty in α and ~0.25% in θ. These uncertainties are considered insignificant for the purpose of the present discussion. The angles derived in Table 2 probably are too low by an amount similar to that of SiO_2 (see also above). In the following discussion, therefore, the relative changes of the *T*–O–*T* angles as a function of bulk composition, and not their absolute values, will be emphasized.

The data in Table 2 suggest that with increasing Al/(Al+Si) the *T*–O–*T* angle in unit I (larger angle) remains constant, whereas that of unit II decreases slightly. The force constants from both units decrease rapidly as a result of the decreased values of W3 and W4 with increasing Al/(Al+Si). The rate of decrease of the force constants may be slightly greater for unit I compared with unit II (Fig. 14). Because the Al–O bond is considerably weaker than that of Si–O, we suggest that this decrease is related to the weakening of the *T*–O–*T* bonds as Al is substituted for Si. The smaller decrease of the *T*–O–*T* angle and slightly more rapid decrease of the force constant of unit II with increasing bulk Al/(Al+Si) may indicate a slight preference of Al for this structural unit (smaller *T*–O–*T* angle) rather than for unit I. This preference accords with the observation that in crystalline framework silicates, the Al–O distance is approximately 10% longer than the Si–O distance (*e.g.*, Smith, 1954; Ribbe *et al.*, 1962).

The systematic increase of intensity of Raman bands associated with unit II (smaller *T*–O–*T* angle) compared with those associated with unit I (larger *T*–O–*T* angle) (Fig. 7) implies that the *average* *T*–O–*T* angle of these melts decreases with increasing Al/(Al+Si). If it is assumed that the two structural units have equal scattering power, a weighted mean *T*–O–*T* angle (θ_{av}) may be calculated by multiplying the angle of the two structural units by the fractional intensity associated with its W4 vibration (*i.e.*, $\theta_{av} = \theta_I A_1/(A_1 + A_2) + \theta_{II} A_2/(A_1 + A_2)$, where indices 1 and 2 refer to the numbering of the lines in Table 2). The average *T*–O–*T* angles thus obtained (Table 2) show a decrease from 130.7° to 124.1° in the compositional range between SiO_2 and $NaAlSiO_4$. This relative change (4.6% relative to the value for SiO_2) compares well with the change obtained from X-ray RDF data by deJong and Brown (1980), Konnert and Karle (1973) and Taylor and Brown (1979b) (5.8%).

By analogy to the spectrum of glassy SiO_2, the band shifting from 903 cm^{-1} in SiO_2 to 854 cm^{-1} in $NaAlSiO_4$ is assigned to a defect in the structural units. Both a bond weakening upon substitution of Al for Si and a decrease in the average *T*–O–*T* angle (*cf.*, Lucovsky, 1979, Table 5) will result in a shifting of the band to lower frequency with increasing Al/(Al+Si) of the melt.

SiO_2–$CaAl_2O_4$ and SiO_2–$MgAl_2O_4$

In the systems SiO_2–$CaAl_2O_4$ and SiO_2–$MgAl_2O_4$ the line frequencies of the bands in the high-frequency envelopes are essentially independent of bulk Al/(Al+Si) (Figs. 3, 10 and 12). The bands characteristic of the end members, *i.e.*, SiO_2 and $CaAl_2O_4$ (Figs. 2 and 9), may be traced, with relative intensities as a function of Al/(Al+Si), into the compositions on the join.

An additional group of bands appears (510–530, 750, 920 and 980 cm^{-1}) with a maximum relative intensity near Al/(Al+Si) = 0.5. We suggest that the latter bands are related to a structural unit with stoichiometry similar to $Al_2Si_2O_8^{2-}$. Results of calculations with the central-force model with a postulated $Al_2Si_2O_8^{2-}$ unit suggest that the 920 cm^{-1} band corresponds to W2; 980 cm^{-1}, to W4; 750 cm^{-1}, to W3; and ~515 cm^{-1}, to W1 in four-membered,

interconnected $Al_2Si_2O_8^{2-}$ rings. These band positions resemble those observed thus indicating that such three-dimensional structures occur in quenched $CaAl_2O_4$–SiO_2 melts.

The similarity of the $CaAl_2O_4$ glass spectrum to that of crystalline $CaAl_2O_4$ (*cf.* Mysen *et al.*, 1981) leads to the suggestion that the $Al_2O_4^{2-}$ units occur in the quenched melt as six-membered rings as in the crystalline phase (Dougill, 1957). For the present discussion the most important bands in the spectrum of $CaAl_2O_4$ glass are those near 780 and 840 cm^{-1} (Fig. 8). The relatively weak band near 820 cm^{-1} in the CATS and CA6S4 spectra may be a composite of the 844 and 775 cm^{-1} bands observed in $CaAl_2O_4$ (Fig. 8). Further evidence for the existence of six-membered $Al_2O_4^{2-}$ rings in melts on the joins SiO_2–$CaAl_2O_4$ and SiO_2–$MgAl_2O_4$ will be derived from the volume relationships discussed below.

We suggest, therefore, that the observed trends in the Raman spectra result from mixtures of SiO_2, $Al_2Si_2O_8^{2-}$ and $Al_2O_4^{2-}$ interconnected, three-dimensional structures in melts on the joins SiO_2–$CaAl_2O_4$ and SiO_2–$MgAl_2O_4$. Their relative proportions, but not their bulk compositions, depend on Al/(Al+Si) of the melt. The data in Figures 10 and 13 show that the three, 3-dimensional species have a considerable overlap in terms of the bulk melt compositions in which they occur. The SiO_2 unit is present, though in small amounts, in all compositions between SiO_2 and $CaAl_2SiO_6$ (CATS). The $CaAl_2O_4$ units occur in the compositional range between $CaAl_2O_4$ and at least $CaAl_2Si_2O_8$. In the system $MgAl_2O_4$–SiO_2, $Al_2O_4^{2-}$ units probably also occur in MA2S2.

The SiO_2 unit with the larger Si–O–Si angle (unit I with characteristic bands at 490, 793 and 1200 cm^{-1}) cannot be detected for melts with Al/(Al+Si) > 0.25 in the Ca system and with Al/(Al+Si) > 0.33 in the Mg system. This observation may indicate that unit I has a slightly broader stability field in the latter system.

Correlation between physical properties and three-dimensional melt structure

In the following subsections the different structural behavior of glasses in the systems SiO_2–$NaAlO_2$, SiO_2–$CaAl_2O_4$ and SiO_2–$MgAl_2O_4$ is related both to the variation of physical properties along these joins and to systematic differences between compositions on different joins. In the following discussion it is considered that the bulk properties of a melt or a glass will depend on (1) the properties of the individual structural units present, (2) the concentrations of these units and (3) the properties of the cation polyhedra of the metal cation acting to charge-balance aluminum in the network.

Volumes

On all three joins investigated here, the density of glasses at room temperature increases with increasing Al/(Al+Si) (Riebling, 1964, 1966; Taylor and Brown, 1979a; see also Table 1). In the system SiO_2–$CaAl_2O_4$, where the data cover the widest range of Al/(Al+Si), the density *vs.* composition relation shows two nearly linear segments. The one with the steeper slope extends from vitreous SiO_2 to the anorthite composition. The one with the shallower slope extends from the anorthite composition to $CaAl_2O_4$ (Fig. 15). By extrapolation to the $CaAl_2O_4$ end member, its estimated density in the vitreous state is 2.85 ± 0.05 g/cm^3.

These density variations may be rationalized in terms of the mixing of SiO_2, $CaAl_2Si_2O_8$ and $CaAl_2O_4$ units. Because the bulk compositional ranges of their coexistence overlap in the central portion of the system, the density *vs.* composition curve probably would not show a sudden discontinuity in slope, but rather a strong curvature in the vicinity of the anorthite composition in agreement with observation. Although only a portion of the compositional range is covered in the system SiO_2–$MgAl_2O_4$ (from $MgAl_2Si_2O_8$ to SiO_2), the segments for which there are data show similar behavior. The density and composition relations in these two systems appear, therefore, to be due to similar effects.

The density data on the join SiO_2–$NaAlO_2$ are too few and scattered for one to reach conclusions similar to that for the join SiO_2–$CaAl_2O_4$. On the basis of their density measurements at room temperature, Taylor and Brown (1979b) derived a nonlinear density relationship with changing Al/(Al+Si), with glass of nepheline composition being less dense than predicted from a linear model. Taylor and Brown (1979b) explained this observation on the basis of increased structural irregularity and a general structural expansion of the framework with increasing Al/(Al+Si). The random Si,Al substitution inferred from the Raman spectra would result in increased *T*–O distance. The data by Taylor and Brown (1979b) are therefore consistent with the present conclusions.

On the basis of the present interpretations of the Raman data some of the minerals precipitating from the melts under consideration have ring structures similar to those of the melts themselves and some

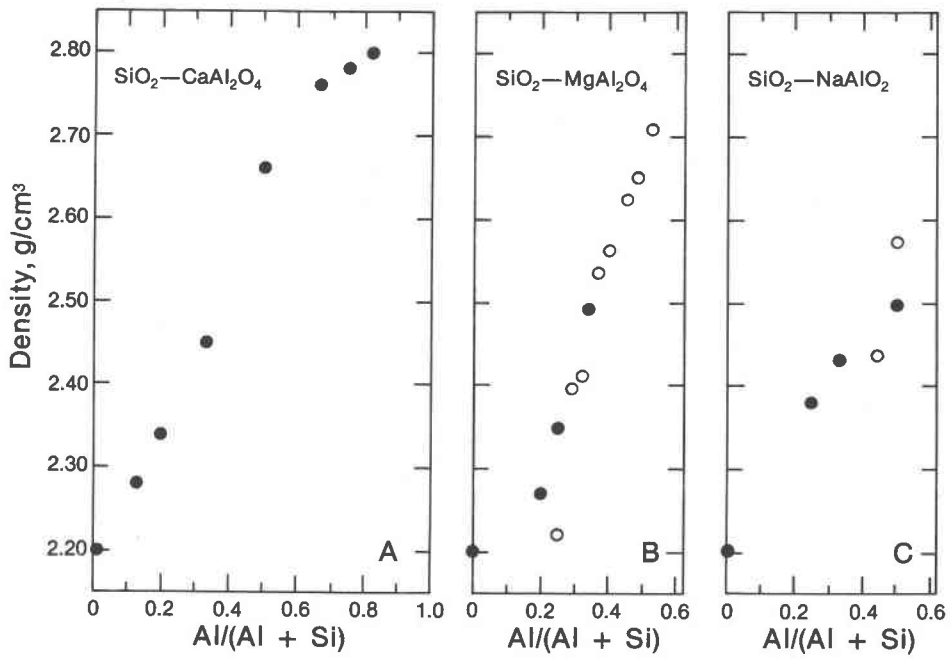

Fig. 15. Density of glasses and melts in the systems SiO_2–$NaAlO_2$, SiO_2–$CaAl_2O_4$ and SiO_2–$MgAl_2O_4$. Dots: Data obtained on glass at room temperature. Open circles: Room-temperature densities calculated from melt expansion measurements. Sources of data: Riebling (1964, 1966), Taylor and Brown (1979b) and Table 1.

differ. It is of interest, therefore, to compare the densities of these glass compositions with their crystalline equivalents. For all samples in which the ring types in the crystal and the melt correspond (that is, cristobalite, tridymite, nepheline and carnegeite with six-membered rings and anorthite with four-membered rings), the density difference between the glass and the mineral is considerably less than for samples in which the ring types do not correspond (Fig. 16). Regression analysis with the inclusion of tridymite, cristobalite, nepheline, carnegeite and anorthite results in the equation:

$$d_{cryst} = 0.92 d_{glass} + 0.25; \qquad r^2 = 0.97.$$

The results indicate a relatively constant difference in packing of the same species in glass *versus* crystal.

Further support for the existence of six-membered rings in vitreous $CaAl_2O_4$ may be derived from considerations similar to those above. The calculated density of $CaAl_2O_4$ glass (from the above equation) is 2.94 g/cm^3, only 3.3% higher than the extrapolated value from the data in Figure 15 (2.85 g/cm^3). For compositions with different ring types in the glass and in the crystals (*e.g.*, K-feldspar and albite), the difference is more than 7%. We suggest, as a result of these data and the suggested interpretation of the Raman spectrum of $CaAl_2O_4$ crystals and glass (Fig. 8; Mysen *et al.*, 1981), that vitreous $CaAl_2O_4$ contains the same type of six-membered rings as the crystalline phase.

In alkali feldspar compositions, the density difference between the vitreous and crystalline state is much greater than for those discussed so far (0.17 g/cm^3 *vs.* a mean of 0.06 g/cm^3). This difference may be related to the difference in ring size of the crystalline and molten aluminosilicate. The four-membered rings of the crystalline phase are more densely packed than the six-membered rings of the glass.

Thermal expansion data are still too scattered and uncertain to be explained on the basis of the anionic structure model of melts and glasses. In the melt region, thermal expansion on the join SiO_2–$MgAl_2O_4$ (Riebling, 1964) is virtually zero from Al/(Al+Si) = 0 to 0.33 and then increases rapidly to a maximum near Al/(Al+Si) = 0.5. This maximum helps to emphasize the uniqueness of this composition where, according to the present structural model, the maximum concentration of $Al_2Si_2O_8^{2-}$ complexes occurs. The nonlinear behavior of thermal expansion between Al/(Al+Si) = 0 and 0.5 may be related to the same causes as the nonlinear density relationships discussed above (Fig. 15).

It is suggested that at high silica contents the thermal expansivity of the melts is predominantly controlled by the expansivity of the siliceous network and not by that of the few interspersed regions containing $Al_2Si_2O_8^{2-}$ complexes. The trends in thermal expansion cannot, however, be generalized on the basis of the anionic model alone. For instance, thermal expansion increases strongly from vitreous SiO_2 to glasses of albite and K-feldspar composition (Arndt and Haberle, 1973), where the structure type does not depend on Al/(Al+Si). On the join SiO_2–$CaAl_2O_4$, on the other hand, the thermal expansion is much less in the same Al/(Al+Si) range. These observations may indicate that the thermal expansion by the metal cation polyhedra (Na^+, K^+ and Ca^{2+}) influences the bulk expansion in addition to the expansion of the three-dimensional anionic units themselves. The relative influence of the melts cannot, at present, be separated.

We speculate that the anomalous behavior of the compressibility of vitreous SiO_2 at room temperature (Bridgman, 1948) and the two-step densification process reported by Arndt and Stoffler (1969) at temperatures below that of the glass transition are related to the two different ring sizes proposed for this composition on the basis of the present data. From considerations of volume it may be expected that the unit with the larger Si–O–Si angle (unit I; Table 2) is more compressible than that with the smaller Si–O–Si angle (unit II; Table 2) and that on increase of pressure, unit I is continuously transformed into unit II. According to this concept, at pressures above about 30 kbar the compressibility of vitreous SiO_2 will be controlled mainly by the smaller compressibility of unit II. Such a decrease in the mean S–O–Si angle with increasing pressure is also consistent with the results from molecular dynamics calculations on vitreous SiO_2 (Woodcock *et al.*, 1976) and with the behavior of crystalline quartz under pressure (Levien *et al.*, 1980).

Compressibility at temperatures below the glass transition appears generally to be higher for the three-dimensional glass structures consisting of six-membered rings than for those that contain large proportions of four-membered rings. For example, a 13% relative increase in density, measured at room-temperature, was observed for vitreous SiO_2 after compaction at 60 kbar and 600° C (Arndt and Stoffler, 1969). An 8.9% compaction was observed for a sample near the albite composition on the join SiO_2–$NaAlO_2$ at 500° C, whereas only a 4.3% compaction was found for anorthite glass (Arndt, 1971). Kushiro (1981) also noted greater compressibility for melts on the join SiO_2–$NaAlO_2$ than for those on the join SiO_2–$CaAl_2O_4$ with similar Al/(Al+Si) to 15 kbar pressure. Furthermore, the compressibility tends to increase with increasing $NaAlO_2/SiO_2$, whereas the reverse is true for increasing $CaAl_2O_4/SiO_2$ (Kushiro, 1976, 1978, 1981).

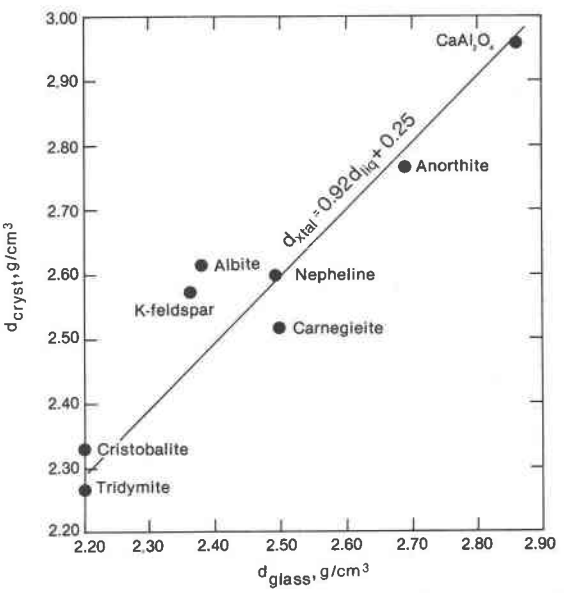

Fig. 16. Density of glass (from Fig. 15) and corresponding minerals (sources of data: Taylor and Brown, 1979a,b; Konnert and Karle, 1973; Dougill, 1957; present data, Table 1).

Viscosity

In the systems Na_2O–Al_2O_3–SiO_2, CaO–Al_2O_3–SiO_2 and MgO–Al_2O_3–SiO_2, the joins SiO_2–$NaAlO_2$, SiO_2–$CaAl_2O_4$ and SiO_2–$MgAl_2O_4$ define lines of maximum viscosity and maxima in activation energies of viscous flow (Riebling, 1964, 1966; Rossin *et al.*, 1964). The viscosity and activation energy of viscous flow decrease in each system on both sides of the joins as the modifier/Al is decreased or increased and nonbridging oxygens are formed (Riebling, 1964, 1966; Mysen *et al.*, 1981a, 1980) at the expense of the three-dimensional network structure. Even along the joins with fully polymerized network structures, however, both the viscosity and the activation energy of viscous flow show a marked dependence on composition and the nature of the charge-balancing cation.

The activation energy of viscous flow decreases with increasing Al/(Al+Si) in all systems (Fig. 17), but at a much slower rate along the join SiO_2–$NaAlO_2$ than along the joins SiO_2–$CaAl_2O_4$ and SiO_2–

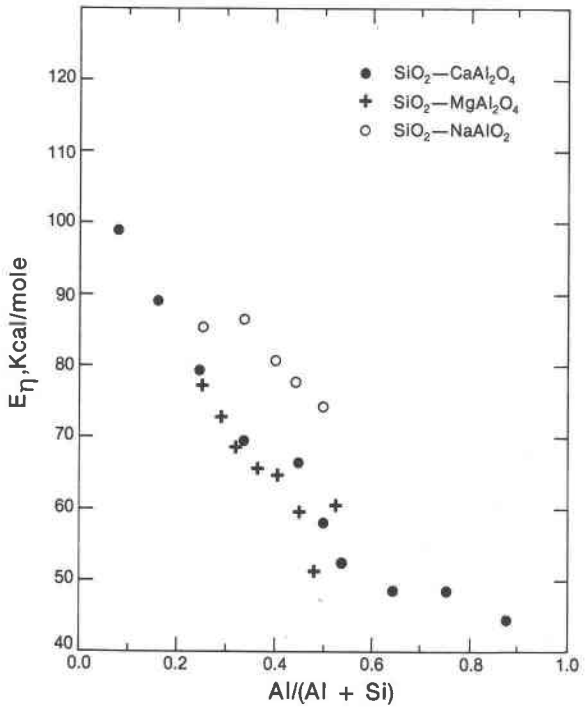

Fig. 17. Activation energies of viscous flow (E_η) in the systems SiO_2–$NaAlO_2$ (Riebling, 1966), SiO_2–$CaAl_2O_4$ (Rossin *et al.*, 1964) and SiO_2–$MgAl_2O_4$ (Riebling, 1964). For discussion see text.

$MgAl_2O_4$. In the system SiO_2–$CaAl_2O_4$ with Al/(Al+Si) $\gtrsim$ 0.5 the activation energy appears independent of Al/(Al+Si) (Rossin *et al.*, 1964). These data may be explained in terms of the structural model for such melts suggested here. In the system SiO_2–$NaAlO_2$ the decrease in activation energy may mainly reflect a weakening of the *T*–O bonds due to the inferred random substitution of Al for Si in the network structure. In systems with divalent charge-balancing cations, on the other hand, where Al-bearing complexes with invariant Al/Si appear to be formed (*e.g.*, $Al_2Si_2O_8^{2-}$), a combined effect of two different processes may be expected. First, the *T*–O bonds in the $Al_2Si_2O_8^{2-}$ complexes probably are longer and weaker than the *T*–O bond in the SiO_2 complexes. Second, it is suggested that a mixture of two rather different units may lead to the formation of smaller flow units with weak interconnection. The latter effect is expected to be nonlinear for the same reasons as discussed above for volume behavior and may be reflected in the concave form of the activation energy versus Al/(Al+Si) at high SiO_2 contents of the melts (Fig. 17). The two effects taken together may also account for the greater rate of decrease of the activation energies of viscous flow with increasing $CaAl_2O_4/SiO_2$ than with increasing $NaAlO_2/SiO_2$.

The nearly constant activation energy of viscous flow for melts in the system SiO_2–$CaAl_2O_4$ with Al/(Al+Si) $\gtrsim$ 0.5 may be explained by the mixing of structural units of subequal activation energies. The slight increase at the highest $CaAl_2O_4$ concentration, although nearly within the uncertainty of the data, might reflect a similar mixing effect, as discussed above for the SiO_2-rich side of the join. The absence of a sharp kink in the activation energy curve at the composition Al/(Al+Si) = 0.5 can be related to the existence of small amounts of the SiO_2-rich network in the more aluminous compositions.

It may not be fortuitous that an extrapolation of activation energies in the system SiO_2–$NaAlO_2$ to Al/(Al+Si) = 1.0 yields a value similar to that of $CaAl_2O_4$ melt. The structures of both melts probably contain six-membered AlO_4 rings. The inferred similar activation energies of viscous flow and the congruence of activation energies in the systems SiO_2–$MgAl_2O_4$ and SiO_2–$CaAl_2O_4$ at constant Al/(Al+Si) lead to the suggestion that the anionic structure plays a dominant role for the activation energies of viscous flow. The charge-balancing cation, according to this concept, plays only a passive role in determining, by its valence, either the formation of six-membered rings with bulk compositionally dependent Al/(Al+Si) or the formation of $Al_2Si_2O_8^{2-}$ complexes.

Thermochemical properties

Flood and Knapp (1968) suggested that the melting behavior of compositions on the joins SiO_2–$CaAl_2Si_2O_8$ and SiO_2–$BaAl_2Si_2O_8$ may be explained by assuming that siliceous and aluminous units coexist in the melt. For the aluminous units, Flood and Knapp (1968) derived a composition $4AlO_2{\cdot}3SiO_2$, which has a slightly higher Al/Si than the unit derived here ($Al_2Si_2O_8^{2-}$) for similar systems. At least a part of this discrepancy may be related to the presence of $Al_2O_4^{2-}$ six-membered rings in addition to the six-membered SiO_2 rings and four-membered $Al_2Si_2O_8^{2-}$ rings in melts of $CaAl_2Si_2O_8$ composition. There is, therefore, essential agreement between the deductions based on the melting behavior in the aluminosilicate system and the conclusions based on Raman spectroscopic information.

The melting behavior of compositions on the joins SiO_2–$NaAlO_2$ and SiO_2–$KAlO_2$ is consistent

with a random substitution of Al for Si (Flood and Knapp, 1968), again in agreement with the structural inferences from the present study. The data on the join SiO_2–$NaAlO_2$, indicating that the absence of an excess mixing enthalpy (Navrotsky *et al.*, 1980) would be expected in the monovalent aluminosilicate melts, are also consistent with the thermochemical data on this join reported by Navrotsky *et al.* (1980). The observed heat of mixing in the system SiO_2–$CaAl_2Si_2O_8$ has been attributed by Navrotsky *et al.* (1980) to a "rearrangement of the aluminosilicate framework." In the light of the present model, this rearrangement would be ascribed to a slight excess of SiO_2 and of a balancing amount of $Al_2O_4^{2-}$ in addition to the stoichiometric proportions indicated by the composition of the melt, as illustrated by, for example, the structure of melt of anorthite composition.

Implications for the structure of magma

On the basis of published bulk chemical analyses of igneous rocks, Mysen *et al.* (1981) found that most such silicate melts have NBO/T < 1. They concluded, therefore, that nearly all igneous melts consist of structural units that, on the average, have NBO/T = 2, 1 and 0. Furthermore, most magmatic liquids have most of the tetrahedral cations made up of Si+Al. It is likely, therefore, that the bulk physical properties of such melts depend strongly on Al/(Al+Si) of the structural units and on the type of metal cation used for charge-balance of Al^{3+} in tetrahedral coordination.

Mysen *et al.* (1981) calculated the distribution of Si and Al between three-dimensional, sheet and chain units in magma (Mysen *et al.*, 1981, Table 10). The present structural model may be used to refine those calculations in terms of the type and proportions of three-dimensional units that occur in magmatic liquids. Calculations (Table 3) have been carried out with the data of Mysen *et al.* (1981) and those in Figures 7, 10 and 13. On the basis of the bulk compositions of the rocks and the spectroscopic data, the three-dimensional network units may be calculated in terms of the structural information from the systems SiO_2–$NaAlO_2$, SiO_2–$CaAl_2O_4$ and SiO_2–$MgAl_2O_4$. In Cenozoic volcanic rocks, from the compilation of Chayes (1971, 1975), it is found that only about 4% of these melts are peralkaline (F. Chayes, personal communication, 1981). Only in this very small proportion of natural melts may the network, therefore, be described with the alkali-aluminosilicate components alone. These observations imply that, provided K^+ and Na^+ play similar roles in these melts, in only about 4% of the cases will there be no six-membered SiO_2 interconnected rings in the magmatic liquid. In the remaining part of natural magma, some Al^{3+} will be balanced with alkaline earths, in which case the magma will contain some Al-free, six-membered SiO_2 rings. In approximately 85% of the magma compositions found in the rock file described by Chayes (1971, 1975; personal communication, 1981), these alkaline earths are Ca^{2+} and Mg^{2+}. In most of these cases, however, the charge-balancing metal cations are only Na^+ and Ca^{2+}.

Table 3. Distribution (percent of total) of types of three-dimensional structural units in some common magma types

	Rhyolite	Dacite	Andesite	Subalkaline basalt
Al/(Al + Si)	0.20	0.23	0.24	0.27
$\underline{M}^+/(\underline{M}^+ + \underline{M}^{2+})$	0.82	0.55	0.47	0.31
$Ca_{0.5}Al^{4+}$(%)	18	45	50	69
$Mg_{0.5}Al^{4+}$(%)	0	0	3	0
Si_4O_8(%)	9	19	23	27
$Al_2Si_2O_8^{2-}$	9	25	27	42
$(Al,Si)_4O_8$(I)	16	11	8	4
$(Al,Si)_4O_8$(II)	66	46	42	27

Bulk rock analyses: averages from Chayes (1975).
Symbols: Al/(Al + Si) = ratio in three-dimensional network (from Mysen et al., 1981a). $\underline{M}^+/(\underline{M}^+ + \underline{M}^{2+})$ = proportion of monovalently charge-balanced Al^{3+} in three-dimensional network. (%) = percent of type relative to total amount of three-dimensional network. (I) and (II) = units I and II in monovalently charge-balanced Al^{3+}-bearing complexes.

It is noted from the examples shown in Table 3 that despite the higher silica contents of andesite, dacite and rhyolite than in basalt, the proportion of Al-free SiO_2 three-dimensional units relative to the total proportion of three-dimensional network units occurring in the magma increases in the more basic magmas. This conclusion is a direct consequence of the greater (Ca+Mg)/(Ca+Mg+Na+K) in basaltic rocks compared with acidic rocks.

In systems with approximately the same Al content, the proportion of Al-free, six-membered SiO_2 rings is positively correlated with the ratio of alkaline earths to alkaline earths + alkali metals. Although the Al/(Al+Si) tends to increase slightly as the basicity of the magma increases (Mysen *et al.*, 1981), the effect of the metal proportions predominates.

On the basis of volume properties of silicate melts discussed above (Figs. 15 and 16), it is suggested that the compressibility of three-dimensional network units in basalt is smaller than in more acidic rocks. Furthermore, in comparing alkali basalt and tholeiite (which have similar NBO/*T*), the alkali basaltic melt will be the most compressible. Inasmuch as the compressibility of binary MO–SiO_2 and M_2O–SiO_2 melts decreases with increasing M/Si (Bockris and Kojonen, 1960), it follows that basic magmas are less compressible than acidic magmas.

It has been shown (Riebling, 1964, 1966; Rossin *et al.*, 1964) that melts on alkaline earth-aluminosilicate joins are less viscous than those with alkali metals. These differences were related to the different ring types discussed above. It may be suggested, therefore, that alkali basalts are likely to be more viscous than tholeiite at the same pressure and temperature. In comparing rocks with different NBO/*T*, Mysen *et al.* (1981a) found a correlated, albeit considerably scattered, relationship between the activation energy of viscous flow of magma and NBO/*T*. They related the scatter to the Al/(Al+Si) of the structural units. In the light of the present data, the variations in Al/(Al+Si) in conjunction with different metal cation proportions control the types of three-dimensional units present and, therefore, probably would better account for the scatter in the relationship between NBO/*T* and the activation energy of viscous flow.

Acknowledgments

Critical reviews by P. Danckwerth, L. W. Finger, P. McMillan, A. Navrotsky and H. S. Yoder, Jr., are appreciated. This research was partially supported by National Science Foundation grant EAR 7911313.

References

Arndt, J. (1971) Densification of glasses of the system Na_2O-CaO–SiO_2–Al_2O_3 by very high static pressures. Naturwissenschaften, 58, 218.

Arndt, J. and Haberle, F. (1973) Thermal expansion and glass transition temperatures of synthetic glasses of plagioclase-like composition. Contributions to Mineralogy and Petrology, 39, 175–183.

Arndt, J. and Stoffler, D. (1969) Anomalous changes in some properties of silica glass densified at very high pressures. Physics and Chemistry of Glasses, 10, 117–124.

Bando, Y. and Ishizuka, K. (1979) Study of the structure of silica glass by high-resolution electron microscopy. Journal of Non-Crystalline Solids, 33, 375–382.

Barker, A. S. and Sievers, A. F. (1975) Optical studies of the vibrational properties of disordered solids. Reviews in Modern Physics, 47, 1–169.

Bates, J. B., Hendricks, R. W., and Shaffer, L. B. (1974) Neutron irradiation effects and the structure of non-crystalline SiO_2. Journal of Chemical Physics, 61, 4163–4176.

Bell, R. J. and Dean, P. (1972) Localization of phonons in vitreous silica and related glasses. In R. W. Douglas and B. Ellis, Eds., International Conference on the Physics of Non-Crystalline Solids, 3rd, University of Sheffield, 1970, p. 443–452. Wiley-Interscience, London.

Bockris, J. O'M., MacKenzie, J. D. and Kitchner, J. A. (1955) Viscous flow in silica and binary silicates. Transactions of the Faraday Society, 51, 1334–1348.

Bockris, J. O'M. and Kojonen, F. (1960) The compressibility of certain molten alkali silicates and borates. Journal of the American Ceramic Society, 82, 4493–4497.

Brawer, S. A. and W. B. White (1975) Raman spectroscopic investigation of the structure of silicate glasses.—I. The binary silicate glasses. Journal of Chemical Physics, 63, 2421–2432.

Brawer, S. A. and White, W. B. (1977) Raman spectroscopic investigation of the structure of silicate glasses. II. Soda-alkaline earth-aluminum ternary and quaternary glasses. Journal of Non-Crystalline Solids, 23, 261–278.

Bridgman, P. W. (1948) Rough compression of 177 substances to 40,000 kg/cm^2. Proceedings of the American Academy of Arts and Sciences, 76, 71–87.

Chayes, F. (1971) Electronic storage, retrieval and reduction of data about chemical composition of common rocks. Carnegie Institution of Washington Year Book, 70, 197–201.

Chayes, F. (1975) Average composition of the commoner volcanic rocks. Carnegie Institution of Washington Year Book, 74, 547–549.

Cranmer, D. and Uhlmann, D. R. (1981) Viscosities in the system albite–anorthite. Journal of Geophysical Research, 86, 7951–7956.

deJong, B. H. W. S. and Brown, G. E. (1980) Polymerization of silicate and aluminate tetrahedra in glasses, melts and aqueous solutions.—I. Electronic structure of $H_6Si_2O_7$, $H_6AlSiO_7^-$, and $H_6Al_2O_7^{2-}$. Geochimica et Cosmochimica Acta, 44, 491–511.

Dougill, M. W. (1957) Crystal structure of calcium monoaluminate. Nature, 180, 292–293.

Flood, H. and Knapp, W. J. (1968) Structural characteristics of liquid mixtures of feldspar and silica. Journal of the American Ceramic Society, 51, 259–263.

Furukawa, T. and White, W. B. (1980) Vibrational spectra and glass structure. Journal of Non-Crystalline Solids, 38 and 39, 87–92.

Furukawa, T., Fox, K. E. and White, W. B. (1981) Raman spectroscopic investigation of the structure of silicate glasses.—III. Raman intensities and structural units in sodium silicate glasses. Journal of Chemical Physics, 75, 3225–3237.

Galeener, F. L. (1979) Band limits and the vibrational spectra of tetrahedral glasses. Physical Review B, 19, 4292–4297.

Galeener, F. L. and Lucvosky, G. (1976) Longitudinal optical vibrations in glasses: GeO_2 and SiO_2. Physical Review Letters, 37, 1474–1478.

Gaskell, P. M. (1975) Construction of a model for amorphous tetrahedral materials using ordered units. Philosophical Magazine, 32, 211–229.

Gaskell, P. M. and Mistry, A. B. (1979) High-resolution transmission electron microscopy of small amorphous silica particles. Philosophical Magazine, 39, 245–257.

Gaskell, P. H. and Tarrant, I. D. (1980) Refinement of a random network model for vitreous silicon dioxide. Philosophical Magazine, B42, 265–286.

Hamilton, W. C. (1965) Significance test of the crystallographic *R* factor. Acta Crystallographica, 18, 502–510.

Hartwig, C. M. (1977) The radiation-induced formation of hydrogen and deuterium compounds in silica as observed by Raman scattering. Journal of Chemical Physics, 66, 227–239.

Hill, R. J. and Gibbs, G. V. (1979) Variation in *d*(*T*–O), *d*(*T*. . . .*T*) and *TOT* in silica and silicate minerals, phosphates and aluminates. Acta Crystallographica, B35, 25–30.

Konnert, J. H. and Karle, L. (1973) The computation of radial distribution functions for glassy materials. Acta Crystallographica, A29, 702–710.

Kushiro, I. (1976) Changes in viscosity and structure of melts of $NaAlSi_2O_6$ composition at high pressures. Journal of Geophysical Research, 81, 6347–6350.

Kushiro, I. (1978) Viscosity and structural changes of albite ($NaAlSi_3O_8$) melt at high pressure. Earth and Planetary Science Letters, 41, 87–91.

Kushiro, I. (1981) Viscosity change with pressure of melts in the system CaO–Al_2O_3–SiO_2. Carnegie Institution of Washington Year Book, 80, 339–341.

Levien, L., Prewitt, C. T., and Weidner, D. J. (1980) Structure and elastic properties of quartz at high pressures. American Mineralogist, 65, 920–930.

Loewenstein, W. (1954) The distribution of aluminum in the tetrahedra of silicates and aluminates. American Mineralogist, 39, 92–96.

Long, D. A. (1977) Raman Spectroscopy. McGraw-Hill, New York.

Lucovsky, G. (1979) Spectroscopic evidence for valence-alternation pair defect states in vitreous SiO_2. Philosophical Magazine, B39, 513–530.

Mammone, J. F., Sharma, S. K. and Nicol, M. F. (1981) Ring structures in silica glass—A Raman spectroscopic investigation. EOS, 62, 425.

Mysen, B. O., Virgo, D. and Scarfe, C. M. (1980) Relations between anionic structure and viscosity of silicate melts—a Raman spectroscopic study. American Mineralogist, 65, 690–710.

Mysen, B. O., Virgo, D., and Kushiro, I. (1981) The structural role of aluminum in silicate melts—a Raman spectroscopic study at 1 atm pressure. American Mineralogist, 66, 678–701.

Mysen, B. O., Finger, L. W., Virgo, D., and Seifert, F. A. (1982a) Curve-fitting of Raman spectra of amorphous materials. American Mineralogist, 67,686–695.

Mysen, B. O., D. Virgo and Seifert, F. A. (1982b). The structure of silica melts: Implications for chemical and physical properties of natural magma. Reviews of Geophysics, in press.

Navrotsky, A., Hon, R., Weill, D. F., and Henry, D. J. (1980) Thermochemistry of glasses and liquids in the systems $CaMgSi_2O_6$–$CaAl_2Si_2O_8$–$NaAlSi_3O_8$, SiO_2–$CaAl_2Si_2O_8$ and SiO–Al_2O_3–CaO–Na_2O. Geochimica et Cosmochimica Acta, 44, 1409–1423.

Ribbe, P. H., Ferguson, R. B., and Taylor, W. H. (1962) A three-dimensional refinement of the structure of low albite. Norsk Geologisk Tidsskrift, 42, 104–138.

Riebling, E. F. (1964) Structure of magnesium silicate liquids at 1700°C. Canadian Journal of Chemistry, 42, 2811–2821.

Riebling, E. F. (1966) Structure of aluminosilicate melts containing at least 50 mole % SiO_2 at 1500°C. Journal of Chemical Physics, 44, 2857–2865.

Rossin, R., Bersan, J., and Urbain, G. (1964) Etude de la viscosite de laitiers liquides appartenant au systeme ternaire SiO_2–Al_2O_3–CaO. Revue des Hautes Temperatures et des Refractaires, 1, 159–170.

Seifert, F. A., Mysen, B. O., and Virgo, D. (1981) Structural similarity of glasses and melts relevant to petrological processes. Geochimica et Cosmochimica Acta, 45, 1879–1884.

Sen, P. N. and Thorpe, M. F. (1977) Phonons in AX_2 glasses: from molecular to band-like modes. Physical Review B, 15, 4030–4038.

Smith, J. V. (1954) A review of the Al–O and Si–O distances. Acta Crystallographica, 7, 479–481.

Soules, T. F. (1979) A molecular dynamic calculation of the structure of sodium silicate glasses. Journal of Chemical Physics, 71, 4570–4578.

Stolen, R. H. and Walrafen, G. E. (1976) Water and its relation to broken bond defects in fused silica. Journal of Chemical Physics, 64, 2623–2631.

Sweet, J. R. and White, W. B. (1969) Study of sodium silicate glasses and liquids by infrared spectroscopy. Physics and Chemistry of Glasses, 10, 246–251.

Taylor, M. and Brown, G. E. (1979a) Structure of mineral glasses—I. The feldspar glasses $NaAlSi_3O_8$, $KAlSi_3O_8$ and $CaAl_2Si_2O_8$. Geochimica et Cosmochimica Acta, 43, 61–75.

Taylor, M. and Brown, G. E. (1979b) Structure of mineral glasses—II. The SiO_2–$NaAlSiO_4$ join. Geochimica et Cosmochimica Acta, 43, 1467–1473.

Taylor, M., Brown, G. E. and Fenn, P. M. (1980) Structure of silicate mineral glasses.—III. $NaAlSi_3O_8$ supercooled liquid at 805°C and the effects of thermal history. Geochimica et Cosmochimica Acta, 44, 109–119.

Taylor, I. D. and Rindone, G. E. (1970) Properties of aluminosilicate glasses: V. Low-temperature viscosities. Journal of the American Ceramic Society, 53, 692–695.

Thorpe, M. F. and Galeener, F. L. (1980) Central-force model for the high-frequency vibrational bands of glasses. Journal of Non-Crystalline Solids, 35–36, 1197–1202.

Verweij, H. (1979a) Raman study of the structure of alkali germanosilicate glasses.—I. Sodium and potassium metagermanosilicate glasses. Journal of Non-Crystalline Solids, 33, 41–53.

Verweij, H. (1979b) Raman study of the structure of alkali germanosilicate glasses.—II. Lithium, sodium and potassium digermanosilicate glasses. Journal of Non-Crystalline Solids, 33, 55–69.

Vukcevitch, M. R. (1972) A new interpretation for the anomalous behavior of vitreous silica. Journal of Non-Crystalline Solids, 11, 25–63.

Woodcock, L. V., Angell, C. A., and Cheeseman, P. (1976) Molecular dynamics studies of the vitreous state: simple ionic systems and silica. Journal of Chemical Physics, 65, 1565–1577.

Manuscript received, August 12, 1981;
accepted for publication, March 8, 1982.